Theses and Dissertations   1. Thesis and Dissertation Collection, all items

2002-06

Design of a voltage tunable broadband quantum well infrared photodetector

Konukbay, Atakan.

Monterey, California. Naval Postgraduate School

http://hdl.handle.net/10945/5896

NAVAL POSTGRADUATE SCHOOL
Monterey, California

THESIS

DESIGN OF A VOLTAGE TUNABLE BROADBAND QUANTUM WELL INFRARED PHOTODETECTOR

by

Atakan Konukbay

June 2002

Thesis Advisor:	Gamani Karunasiri
Second Reader:	James Luscombe

Approved for public release; distribution is unlimited

THIS PAGE INTENTIONALLY LEFT BLANK

REPORT DOCUMENTATION PAGE			*Form Approved OMB No. 0704-0188*
Public reporting burden for this collection of information is es timated to average 1 hour per response, including the time for reviewing instruction, searching existing data sources, gathering and maintaining the data needed, and completing and reviewing the collection of information. Send comments regarding this burden estimate or any other aspect of this collection of information, including suggestions for reducing this burden, to Washington headquarters Services, Directorate for Information Operations and Reports, 1215 Jefferson Davis Highway, Suite 1204, Arlington, VA 22202-4302, and to the Office of Management and Budget, Paperwork Reduction Project (0704-0188) Washington DC 20503.			
1. AGENCY USE ONLY *(Leave blank)*	**2. REPORT DATE** June 2002	**3. REPORT TYPE AND DATES COVERED** Master's Thesis	
4. TITLE AND SUBTITLE: Design Of A Voltage Tunable Broadband Quantum Well Infrared Photodetector			**5. FUNDING NUMBERS**
6. AUTHOR(S) Atakan Konukbay			
7. PERFORMING ORGANIZATION NAME(S) AND ADDRESS(ES) Naval Postgraduate School Monterey, CA 93943-5000			**8. PERFORMING ORGANIZATION REPORT NUMBER**
9. SPONSORING /MONITORING AGENCY NAME(S) AND ADDRESS(ES) N/A			**10. SPONSORING/MONITORING AGENCY REPORT NUMBER**
11. SUPPLEMENTARY NOTES The views expressed in this thesis are those of the author and do not reflect the official policy or position of the Department of Defense or the U.S. Government.			
12a. DISTRIBUTION / AVAILABILITY STATEMENT Approved for public release; distribution is unlimited			**12b. DISTRIBUTION CODE**
13. ABSTRACT *(maximum 200 words)* The purpose of this thesis is to design a quantum well infrared detector with tunable spectral bandwidth. The tunability of the bandwidth is achieved by using the linear Stark effect for the ground to first excited state transition in an asymmetric quantum well. The position of the absorption peak is dependent on the direction of the electric field, and therefore it can be either blue or red shifted by changing the direction of the field. If two identical asymmetric quantum wells are arranged opposite each other, we can obtain both the blue and red shift for either direction of the bias. This method can produce broader peaks with tunable bandwidths proportional to the applied field. A program was developed to calculate the energy levels and wavefunctions of an arbitrary quantum well. The program was used to design a step quantum well capable of detecting infrared in the 8-12 μm band. The validity of the approach was verified by comparison with experimental data and found to have a good agreement. The designed step well was used to create a tunable bandwidth detector. The analysis showed that the bandwidth could be tuned to more than twice the peak width. The numerical simulation indicates the possibility of manufacturing a tunable bandwidth infrared detector by using step quantum wells.			
14. SUBJECT TERMS Voltage tunable, broadband, quantum well infrared photodetector, "staircase" method, transfer matrix.			**15. NUMBER OF PAGES** 73
			16. PRICE CODE
17. SECURITY CLASSIFICATION OF REPORT Unclassified	**18. SECURITY CLASSIFICATION OF THIS PAGE** Unclassified	**19. SECURITY CLASSIFICATION OF ABSTRACT** Unclassified	**20. LIMITATION OF ABSTRACT** UL

THIS PAGE INTENTIONALLY LEFT BLANK

DESIGN OF A VOLTAGE TUNABLE BROADBAND QUANTUM WELL INFRARED PHOTODETECTOR

Atakan Konukbay
First Lieutenant, Turkish Army
B.S., Turkish Army Academy, 1996

Submitted in partial fulfillment of the
requirements for the degree of

MASTER OF SCIENCE IN APPLIED PHYSICS

from the

NAVAL POSTGRADUATE SCHOOL
June 2002

Author: Atakan Konukbay

Approved by: Gamani Karunasiri
Thesis Advisor

James Luscombe
Second Reader

William B. Maier II
Chairman, Department of Physics

THIS PAGE INTENTIONALLY LEFT BLANK

ABSTRACT

The purpose of this thesis is to design a quantum well infrared detector with tunable spectral bandwidth. The tunability of the bandwidth is achieved by using the linear Stark effect for the ground to first excited state transition in an asymmetric quantum well. The position of the absorption peak is dependent on the direction of the electric field, and therefore it can be either blue or red shifted by changing the direction of the field. If two identical asymmetric quantum wells are arranged opposite each other, we can obtain both the blue and red shift for either direction of the bias. This method can produce broader peaks with tunable bandwidths proportional to the applied field.

A program was developed to calculate the energy levels and wavefunctions of an arbitrary quantum well. The program was used to design a step quantum well capable of detecting infrared in the 8-12 μm band. The validity of the approach was verified by comparison with experimental data of Martinet *et al.* (Martinet, 1992), and found to have a good agreement. The designed step well was used to create a tunable bandwidth detector. The analysis showed that the bandwidth could be tuned to more than twice the peak width. The numerical simulation indicates the possibility of manufacturing a tunable bandwidth infrared detector by using step quantum wells.

THIS PAGE INTENTIONALLY LEFT BLANK

TABLE OF CONTENTS

THIS PAGE INTENTIONALLY LEFT BLANK

LIST OF FIGURES

THIS PAGE INTENTIONALLY LEFT BLANK

LIST OF TABLES

THIS PAGE INTENTIONALLY LEFT BLANK

LIST OF SYMBOLS

A	area of the device
A_n, B_n	wavefunction coefficients in the nth layer
c	speed of light
e	charge of an electron
$\hat{\mathbf{e}}$	electric polarization unit vector
E	energy
E_n	electron energy in the nth energy level
E_f	electron energy in the final state
E_g	energy gap
E_i	electron energy in the initial state
F	external electric field
L	width of the quantum well
$g(\hbar \mathbf{w})$	Lorentzian function
$\hbar$	reduced Plank's constant
I	incident photon flux
$\mathbf{k}$	transverse wave vector
k_n	wave vector in the nth layer
m_b^*	barrier effective mass
m_e^*	effective mass of the electron
$\mathbf{M}_n$	transfer matrix in the nth layer
m_n^*	effective mass in the nth layer
N	number of electrons in the initial state
N_d	three dimensional doping density
n_r	index of refraction
l	length of the region used for the normalization of the extended state wavefunction

u_i	Bloch functions of the initial state
u_f	Bloch functions of the final state
$\vec{p}$	momentum operator
$\mathbf{r}$	3-D position vector
$V(z)$	potential height
V_n	potential height in the nth layer
V_p	interaction potential energy
W	transition rate
x	molar percentage
z	growth direction
z_n	spatial coordinate of the interface between n^{th} and $(n+1)^{th}$ layers
$a(\hbar w)$	absorption coefficient
Γ	full width half maximum value of the excited state
q	the angle between the photon polarization angle and the z axis
e_0	electric permittivity
$r(E)$	joint density of states
Ψ_n	wavefunction in the nth energy level
Ψ_i	envelope functions of the initial state
Ψ_f	envelope functions of the final state
w	angular frequency
$d(x)$	Dirac delta funtion
ΔE_c	band offset of the conduction band
ΔE_v	band offset of the valence band
ΔE_g	total band offset

ACKNOWLEDGMENTS

THIS PAGE INTENTIONALLY LEFT BLANK

I. INTRODUCTION

A. INFRARED DETECTORS

The human eye can detect only a small segment of the electromagnetic spectrum, the familiar visible band ranging from blue to red. Only objects hot enough to radiate at these frequencies and those that reflect visible light are visible to the eye. For the most part, however, objects are too cold to glow noticeably, making them undetectable at night. Yet their finite temperature does give them an infrared glow. It is this glow that night-vision infrared cameras strive to see. At the heart of an infrared camera is its "eye": a two-dimensional array of detector pixels, with each pixel converting some of the incident photons to an electric signal.

A Quantum Well Infrared Photodetector (QWIP) consists of a stack of quantum wells designed to detect infrared light (Levine, 1993). When the quantum well is adequately deep and narrow, its energy states are quantized. The potential depth and width of the well can be adjusted so that it has only two energy states: a ground state near the well bottom and a first excited state near the well top. In Figure 1.1, photoexcited electron transition from the ground state to the first excited state, where an externally applied voltage sweeps them out, producing a photocurrent.
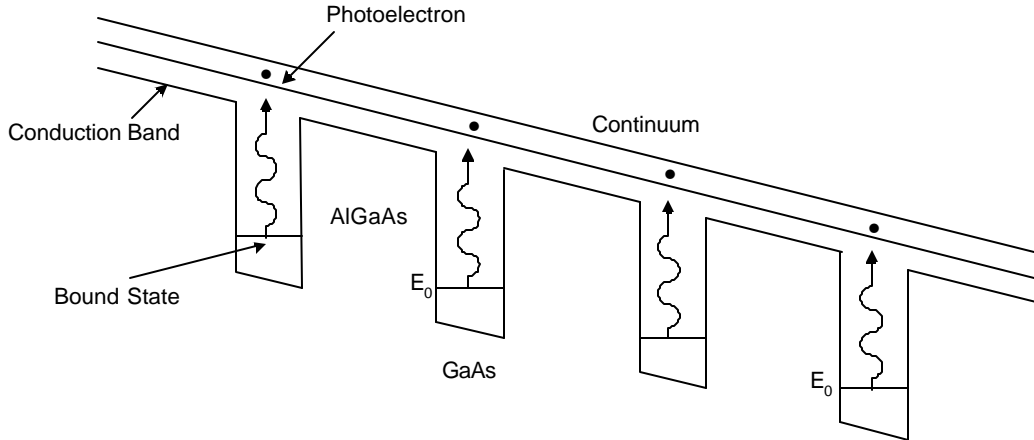
Figure 1.1 Electron excitation of a quantum well infrared photodetector.

For two bound states in the quantum well, only photons having energies corresponding to the energy separation between the two states are absorbed, resulting in a

detector with a sharp absorption spectrum. If there is only one bound state in the well, the transition occurs between the bound state and the continuum, producing a broader peak (Levine, 1993). Designing a quantum well to detect light of a particular wavelength becomes a straightforward matter of adjusting the potential depth and width of the well to produce two states, separated by the desired photon energy. Impressive advances in the crystal growth and processing techniques of compound semiconductors such as gallium arsenide ($GaAs$) and aluminum gallium arsenide ($Al_xGa_{1-x}As$) with different aluminum compositions allowed the fabrication of novel QWIP detectors (Levine, 1993) and arrays (Gunapala, 1996).

B.   PROGRESS OF QWIPS

In the 1970's, InSb and HgCdTe were used to cover the 3-5 and 8-12 micrometer wavelength ranges. However, HgCdTe has some shortcomings due to difficulty in its material preparations, uniformity and reproducibility in the fabrication process. Other difficulties include mechanical softness, sensitivity to elevated temperature, and low yield for large array fabrications, which make such detectors extremely expensive. In order to fabricate low-cost detectors and overcome the above difficulties, detection using superlattices was suggested by Esaki and Tsu (Esaki, 1969). Extensive investigations, both theoretical (Coon, 1984 and 1985) and experimental (Smith, 1983), were a subject of considerable interest and were carried out until the first observation of strong intersubband transitions in $GaAs/AlGaAs$ quantum wells by West and English (West, 1985). Since the problems associated with material preparation were avoided, this new development has received considerable attention.

The first bound-to-bound quantum well infrared photodetector was demonstrated by Levine *et al.* (Levine, 1987). Because the photoelectrons had to tunnel out of wells from the bound excited state under large barriers, as illustrated in Figure 1.2(a), the responsivity was so low that the device had to work using a CO_2 laser. This low responsivity led to the use of bound-to-continuum transitions, which were first proposed by Coon and Karunasiri in 1984 (Coon, 1984). Hasnain *et al.* (Hasnain, 1989)

demonstrated the first bound-to-continuum QWIP (see Figure 1.2b) to have a much higher responsivity, but also a small peak absorbance due to broad spectral width.
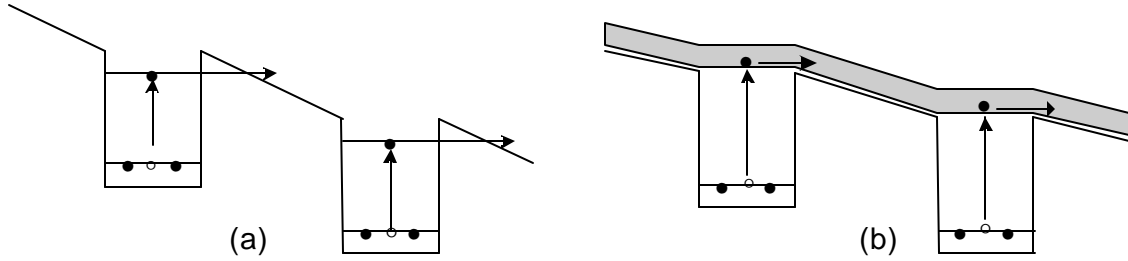
Figure 1.2   Schematic diagrams showing (a) bound-to-bound and (b) bound-to-continuum electron transfer.

Several configurations of the QWIP structure have been reported based on transitions from bound-to-extended states (Levine, 1990), bound-to-quasi-continuum states (Levine, 1991), bound-to-quasibound states (Gunapala, 1996), and bound-to-miniband states (Yu, 1991). These configurations provide good detection performance because in all designs, electrons in the ground state do not flow in response to the bias, while electrons activated to the excited state yield photocurrent under low bias. Several structural optimizations have also been made to improve the performance of QWIPs such as dark current reduction from thermionic emission (Gunapala, 1996).

C.   PURPOSE OF THIS THESIS

The goal of this research is to design a quantum well detector with a tunable spectral bandwidth. The tunability of the bandwidth is achieved by using "the linear Stark effect" in an asymmetric quantum well (Yuh, 1989). For example, in the step quantum well shown in Figure 1.3(a), the amount of Stark shift from the ground to first excited states transition is approximately $\dfrac{eFa}{2}$, where F is the electric field strength, and a is the step width (Yuh, 1989).
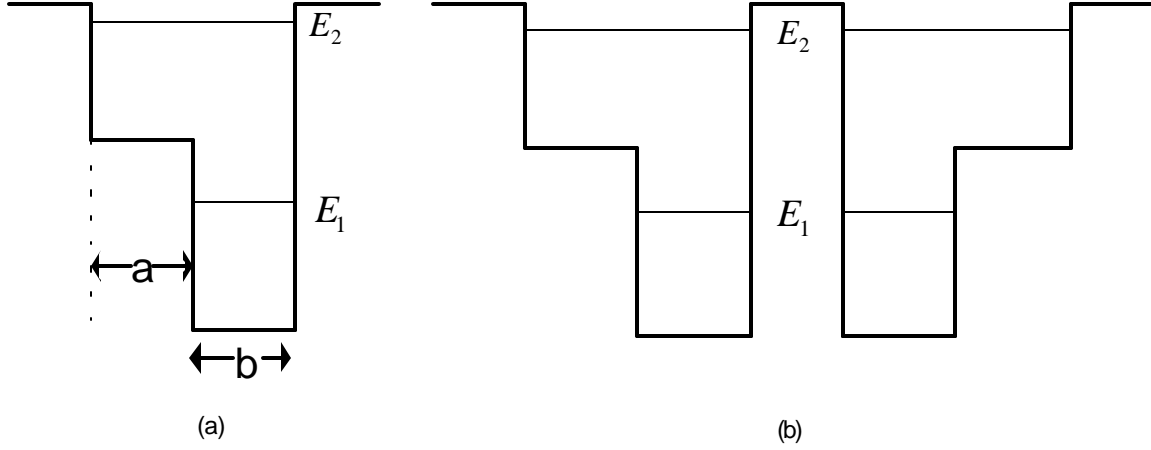
Figure 1.3   Schematic diagrams showing an (a) asymmetric step quantum well and a (b) designed step quantum well structure for bandwidth tuning.

As previously mentioned, the position of the absorption peak is sensitive to the direction of the electric field and can be either blue or red shifted by changing the direction of the field (Mii, 1988). If two wells are arranged as in Figure 1.3(b), both red and blue shifts can occur at the same time producing an absorption peak with a tunable bandwidth.

In the following chapter, we will present a detailed analysis of energy levels in a step quantum well, including external electric field effects. In addition, the absorption coefficient under applied field will be calculated using a step approximation to the linear potential. Finally, in Chapter 3, we will present an optimized device structure to achieve tunable bandwidth detection.

4

II.   THEORETICAL BACKGROUND

A.   INTRODUCTION

In the following sections, we will develop the theoretical tools necessary to analyze quantum well energy levels as a function of applied bias for an asymmetric quantum well. The Schrödinger equation is solved numerically using the transfer matrix approach (Wang, 1989). The effect of the electric field on the energy levels will be incorporated by the "staircase" approximation of the linear potential.

B.   TRANSFER MATRIX METHOD

In the case of an infinite square quantum well, the Schrödinger equation is given by

$$-\frac{\hbar^2 d^2 \Psi_n}{2m_e^* dz^2} = E_n \Psi_n \qquad n = 1,2,3,... \qquad (2.1)$$

where z is the growth direction, n is the quantum number, $\hbar$ is the reduced Planck's constant, m_e^* is the effective mass of the electron, and Ψ_n and E_n are the wavefunction and energy in the nth energy level, respectively. The wave function ? must also satisfy boundary conditions across a potential step since the probability current across a boundary should be continuous.

In light of the above the conditions and the fact that the wave functions go to zero at the boundaries $(z = 0, L)$ and the electron stays within the well, we can obtain the energy and wavefunction of the quantized energy states as

$$E_n = n^2 \frac{\hbar^2 \boldsymbol{p}^2}{2m_e^* L^2} \qquad n = 1,2,3,... \qquad (2.2)$$

and

$$\Psi_n(z) = A\sin\left(\frac{n\boldsymbol{p}z}{L}\right) \qquad n = 1,2,3,... \qquad (2.3)$$

5

where L is the width of the quantum well. Taking the origin at the left side of the well as shown in Figure 2.1, the wave function can then be normalized over the total distance $-\infty < z < +\infty$ as follows:

$$\int_{-\infty}^{\infty} \Psi_n^*(z)\Psi_n(z)dz = 1,$$ (2.4)

which gives the normalization constant $A = \sqrt{\dfrac{2}{L}}$. Finally the normalized wavefunction is given by

$$\Psi_n(z) = \sqrt{\frac{2}{L}}\sin\left(\frac{n\boldsymbol{p}z}{L}\right) \qquad n = 1,2,3,...$$ (2.5)
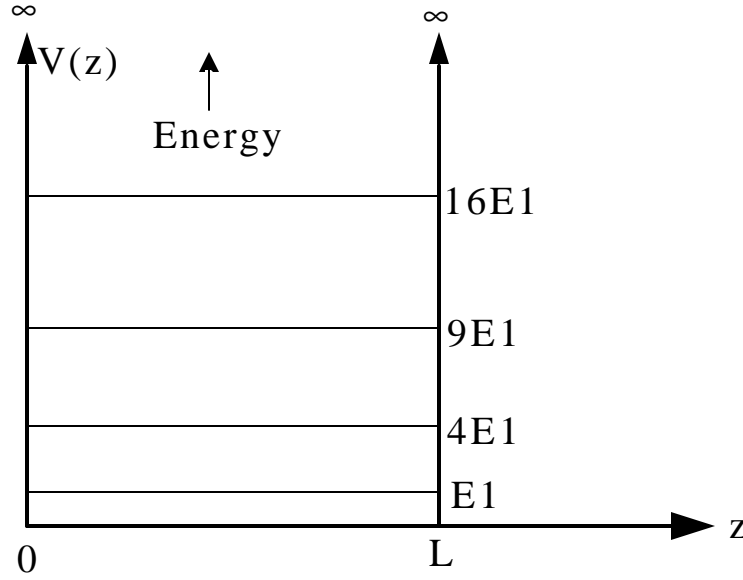
Figure 2.1   Infinite square well potential and energy levels.

There are many techniques available to calculate the energy levels and the wave-functions of finite quantum well structures, each having advantages and disadvantages. The deciding factor on which method to use depends on, to some extent, the structure itself. For example, the variational approach yields simple results for the ground state but has difficulty finding the excited states. The solution of the Schrödinger equation for a finite square quantum well can be found by matching boundary conditions (Weisbuch, 1991). However, when the number of interfaces is large, this method becomes

6

cumbersome (Choi, 1997). With the help of a computer, the transfer-matrix method is a multipurpose approach in obtaining the energy states and the corresponding wave functions of a structure with an arbitrary potential profile. In the following section, the transfer matrix method will be discussed.

A heterostructure is made from layers of materials having different bandgaps. For example, in a typical square quantum well, a layer of $GaAs$ is surrounded between the two thicker higher bandgap layers of $Al_xGa_{1-x}As$. The well width is controlled by adjusting the $GaAs$ layer thickness while the potential depth is controlled by adjusting the Al composition in the barrier layers. Again the application of the boundary conditions leads to the quantized energy values E_n and wave functions $\Psi_n(z)$.

In the transfer matrix method, a plane wave is assumed to be incident from the left of the structure as shown in Figure 2.2. In each layer the wave function can be written as a linear combination of the forward ($A_n e^{ikz}$) and backward ($B_n e^{-ikz}$) traveling plane waves. A matrix can be set up using the boundary conditions at each interface of the quantum well structure to connect the wavefunctions between the adjacent regions (Hutchings, 1989).
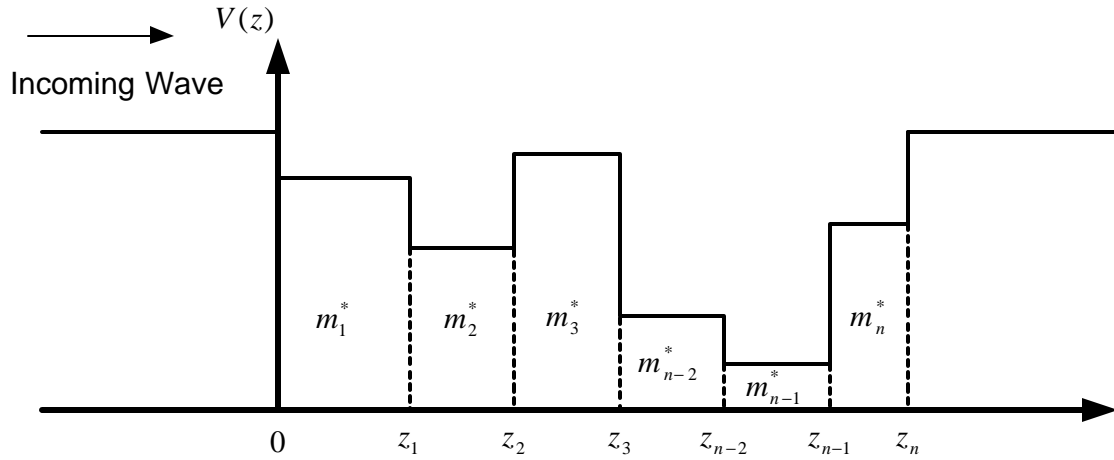
Figure 2.2   Arbitrary multi-layered potential well structure.

For the arbitrary quantum well structure shown in Figure 2.2, the wave function for the nth region can be written as

$$\mathbf{y}_n(z) = A_n e^{i k_n z} + B_n e^{-i k_n z} \qquad n = 1, 2, \ldots, N \tag{2.6}$$

where A_n and B_n are arbitrary constants,

$$k_n = \sqrt{\frac{2m_n^*}{\hbar^2}(E - V_n)}, \tag{2.7}$$

m_n^* is the electron effective mass in the nth layer and the thickness of the nth layer $d_n = z_{n+1} - z_n$. Furthermore, E is the electron energy, which can either be higher or lower than the highest potential in the structure. The boundary conditions at the nth interface give (Robinett, 1997)

$$\mathbf{y}_n(z_n) = \mathbf{y}_{n+1}(z_n)$$

$$\frac{1}{m_n^*} \frac{d\mathbf{y}_n(z_n)}{dz_n} = \frac{1}{m_{n+1}^*} \frac{d\mathbf{y}_{n+1}(z_n)}{dz_n}. \tag{2.8}$$

Thus, the following matrix, M_n, can be obtained to connect the coefficients in the nth layer to that of the $(n+1)^{th}$ layer as follows:

$$\begin{bmatrix} A_{n+1} \\ B_{n+1} \end{bmatrix} = \mathbf{M}_n \begin{bmatrix} A_n \\ B_n \end{bmatrix} \qquad n = 1, 2, \ldots, n-1 \tag{2.9}$$

where

$$\mathbf{M}_n = \frac{1}{2} \begin{bmatrix} (1+\mathbf{g}_n)e^{i(k_n - k_{n+1})z_n} & (1-\mathbf{g}_n)e^{-i(k_n + k_{n+1})z_n} \\ (1-\mathbf{g}_n)e^{i(k_n + k_{n+1})z_n} & (1+\mathbf{g}_n)e^{-i(k_n - k_{n+1})z_n} \end{bmatrix}, \tag{2.10}$$

and

$$\mathbf{g}_n = \frac{k_n m_{n+1}^*}{k_{n+1} m_{n+1}^*}, \tag{2.11}$$

In Equation (2.10) z_n is the spatial coordinate of the interface between n^{th} and $(n+1)^{th}$ layers.

This model can be extended to the multi-layered quantum well structure and by using the above relationship, the coefficients of the wavefunctions for the first and last layers are related by

$$\begin{bmatrix} A_N \\ B_N \end{bmatrix} = \mathbf{M}_n \mathbf{M}_{n-1} \ldots \mathbf{M}_2 \mathbf{M}_1 \begin{bmatrix} A_1 \\ B_1 \end{bmatrix} = \mathbf{M} \begin{bmatrix} A_1 \\ B_1 \end{bmatrix} = \begin{bmatrix} m_{11} & m_{12} \\ m_{21} & m_{22} \end{bmatrix} \begin{bmatrix} A_1 \\ B_1 \end{bmatrix}. \tag{2.12}$$

8

If the two outer layers have higher potentials than the energy of the particle (i.e., if $E < V$), then there will be bound energy states. In this case, we can set the coefficient $B_N = 0$, because it would become infinite as $z \to \infty$. In the same manner, A_1 can be set to zero for the region $z < 0$. Under these conditions, Equation 2.12 reduces to

$$\begin{bmatrix} A_n \\ 0 \end{bmatrix} = \begin{bmatrix} m_{11} & m_{12} \\ m_{21} & m_{22} \end{bmatrix} \begin{bmatrix} 0 \\ B_1 \end{bmatrix}. \tag{2.13}$$

In order to satisfy the Equation 2.13, we must have

$$m_{22}(E) = 0. \tag{2.14}$$

A Matlab program was developed to plot $m_{22}(E)$ versus E and identify the points where m_{22} is zero. For example, Figure 2.3 shows the calculated m_{22} as a function of E for a square potential well. The calculated bound state energies and wavefunctions are shown in Figure 2.4.
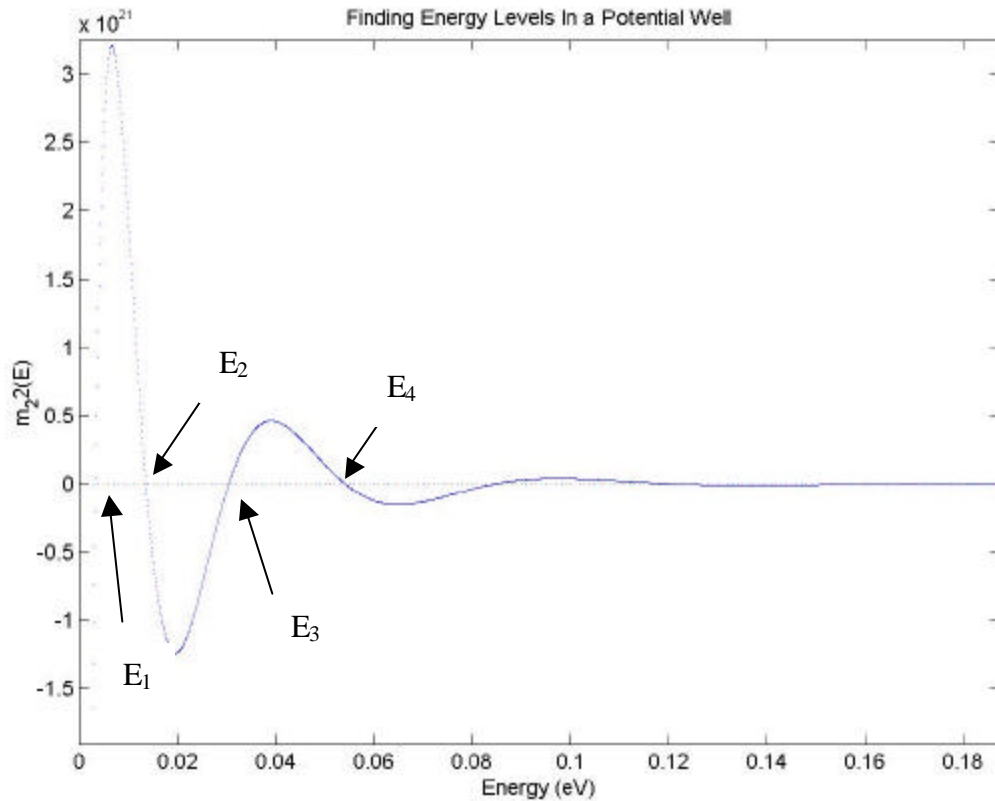
Figure 2.3   Plot of $m_{22}(E)$ versus E for a square potential well with $L = 110$ Å, $V_1 = V_3 = 0.75 \ eV$ and $V_2 = 0 \ eV$.

9
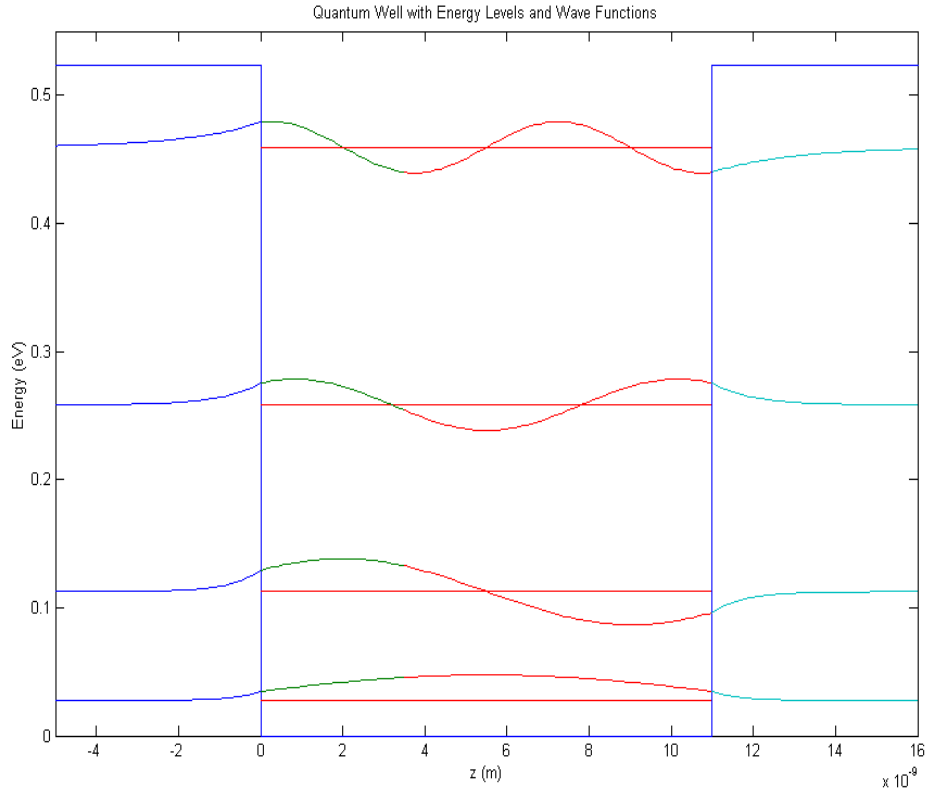
Figure 2.4   Energy levels and wavefunctions of the quantum well described
in Figure 2.3.

C.   INTERSUBBAND TRANSITIONS

In a quantum well structure made of semiconductors, the wavefunction consists of both envelope and Bloch functions. Thus, not only the transitions between Bloch functions but also between the envelope states are allowed within the structure. The transitions between Bloch states correspond to interband transitions, while transitions between envelope states correspond to intersubband transitions. For a given interaction potential V_p, the transition rate W can be obtained from the Fermi's golden rule (Coon, 1984)

$$W = \frac{2p}{\hbar} \sum_f |< \Psi_f \,|\, V_p \,|\, \Psi_i >|^2 \, d \left(E_f - E_i - \hbar w \right),$$ (2.15)

10

where E_i and E_f are the electron energies in the initial and final states, respectively, and $\hbar w$ is the incident photon energy. The interaction potential energy, V_p, in the dipole approximation is given by (Coon, 1984)

$$V_p = \frac{e}{m_e^*} \left(\frac{I\hbar}{2\boldsymbol{e}_0 n_r \boldsymbol{w} c} \right)^{1/2} \hat{\mathbf{e}} \cdot \vec{p} ,$$ (2.16)

where e is the electron charge, I is the incident photon flux, c is the speed of light, $\boldsymbol{e}_0$ is the electric permittivity, n_r is the index of refraction, $\boldsymbol{w}$ is the angular frequency of the incident photon, $\hat{\mathbf{e}}$ is the unit vector of the photon polarization direction, and $\vec{p}$ is the momentum operator,

$$\vec{p} = -i\hbar \left(\vec{i} \frac{\partial}{\partial x} + \vec{j} \frac{\partial}{\partial y} + \vec{k} \frac{\partial}{\partial z} \right).$$ (2.17)

In the case of a quantum well, the wavefunctions for the initial and final states of transition can be written as

$$\Psi_i = u_i(\mathbf{r}) \frac{e^{i\mathbf{k}\cdot\vec{r}}}{\sqrt{A}} \boldsymbol{y}_i(z)$$

$$\Psi_f = \frac{1}{\sqrt{A}} u_f(\mathbf{r}) \frac{e^{i\mathbf{k}\cdot\vec{r}}}{\sqrt{A}} \boldsymbol{y}_f(z) ,$$ (2.18)

where u_i and u_f are the Bloch functions of the initial and final states, respectively, $\vec{k}_i$ and $\vec{k}_f$ are the initial and final wave vectors in the xy plane, $\mathbf{r}$ is the 3-D position vector, $\vec{r}$ is the position vector in the xy plane, Ψ_i and Ψ_f are the corresponding envelope functions, and A is the area of the structure. The transition matrix element in Equation 2.15 can be evaluated as (Coon, 1984)

$$< \Psi_f |V_p| \Psi_i > = < u_f(\mathbf{r})\mathbf{y}_f(z)\frac{e^{i\mathbf{k}_f \cdot \vec{r}}}{\sqrt{A}} |V_p| u_i(\mathbf{r})\mathbf{y}_i(z)\frac{e^{i\mathbf{k}_i \cdot \vec{r}}}{\sqrt{A}} >$$

$$= < u_f(\mathbf{r})e^{i\mathbf{k}_f \cdot \vec{r}} |V_p| u_i(\mathbf{r})e^{i\mathbf{k}_i \cdot \vec{r}} >< \mathbf{y}_f(z)|\mathbf{y}_i(z)> \qquad (2.19)$$

$$+ < \mathbf{y}_f(z)\frac{e^{i\mathbf{k}_f \cdot \vec{r}}}{\sqrt{A}} |V_p| \mathbf{y}_i(z)\frac{e^{i\mathbf{k}_i \cdot \vec{r}}}{\sqrt{A}} >< u_f(\mathbf{r})|u_i(\mathbf{r}) >.$$

In the above expression, we assume that the envelope functions vary slowly compared to the Bloch functions. The integration over the x and y coordinates gives $\vec{k}_i = \vec{k}_f$. The first term of Equation 2.19 is zero because of the fact that the Hamiltonian used to obtain $\mathbf{y}_i$ and $\mathbf{y}_f$ is Hermitian. In addition, the Bloch functions are normalized to unity. Thus, the intersubband transition matrix element reduces to (Coon, 1984)

$$< \Psi_f |V_p| \Psi_i > = < \mathbf{y}_f(z)|V_p|\mathbf{y}_i(z) >$$

$$= \frac{q}{m_e^*}\left(\frac{I\hbar}{2e_0 n_r \mathbf{w}}\right)^{1/2} < \mathbf{y}_f(z)|P_z|\mathbf{y}_i(z) > \cos\mathbf{q}, \qquad (2.20)$$

where $\mathbf{q}$ is the angle between the photon polarization angle and the z axis and P_z is the momentum operator in the z direction. The strength of the transition is usually characterized by the oscillator strength, which is defined as

$$f = \frac{2m_e^*(E_2 - E_1)}{\hbar^2}\left|\left\langle \Psi_f | z | \Psi_i \right\rangle\right|^2, \qquad (2.21)$$

where

$$\left\langle \Psi_f | z | \Psi_i \right\rangle = \int_{-\infty}^{\infty} \Psi_f \, z \, \Psi_i \, dz. \qquad (2.22)$$

D.   INTERSUBBAND TRANSITION SELECTION RULES

The first selection rule of intersubband transition is the parity selection rule. From Equation 2.20, it is found that the parity of the final state has to be different from that of the initial state in order to obtain a non-zero transition matrix element. This means that

the intersubband transitions in a square quantum well can occur only from odd states to even states or vice versa. For example $1 \rightarrow 2$ or $2 \rightarrow 3$ transitions are allowed whereas $1 \rightarrow 3$ is not allowed. Figure 2.5 shows schematically the parity selection rule of the intersubband transitions in a square potential well. However, the symmetry of a square well can be broken by applying a relatively strong electric field, making the normally "forbidden" transitions become allowed (Mii, 1990).
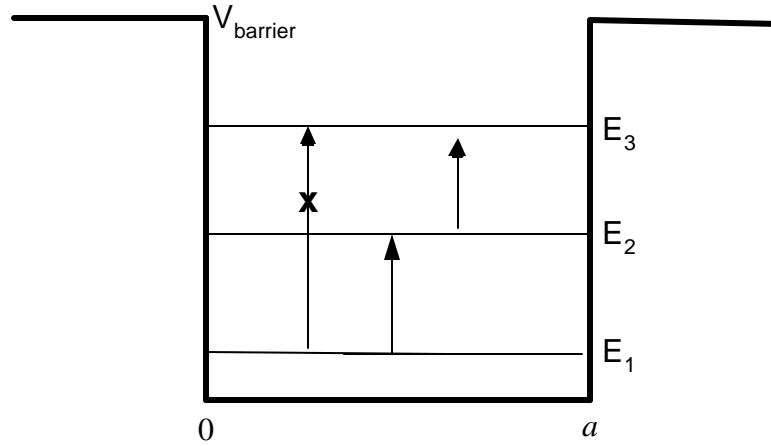
Figure 2.5   Square quantum well showing allowed and forbidden transitions.

The second selection rule is the polarization selection rule. Since the potential modulation of a quantum well structure is only in one direction, the z direction, intersubband transition will not occur when the photon polarization is perpendicular to the z direction. This can be understood by considering the $\cos\boldsymbol{q}$ term in Equation 2.20. This unique polarization selection rule is an important characteristic and can be used for the identification of the intersubband transition (West, 1985). In order to obtain a strong intersubband transition, the photon polarization has to coincide with the growth direction (i.e., $\boldsymbol{q} = 0$).

For an asymmetric quantum well (see Figure 2.6), the dipole matrix elements of transitions for both odd-to-odd and even-to-even quantum numbers do not vanish, since the eigenfunctions of these energy states are not eigenfunctions of the parity operator.

13
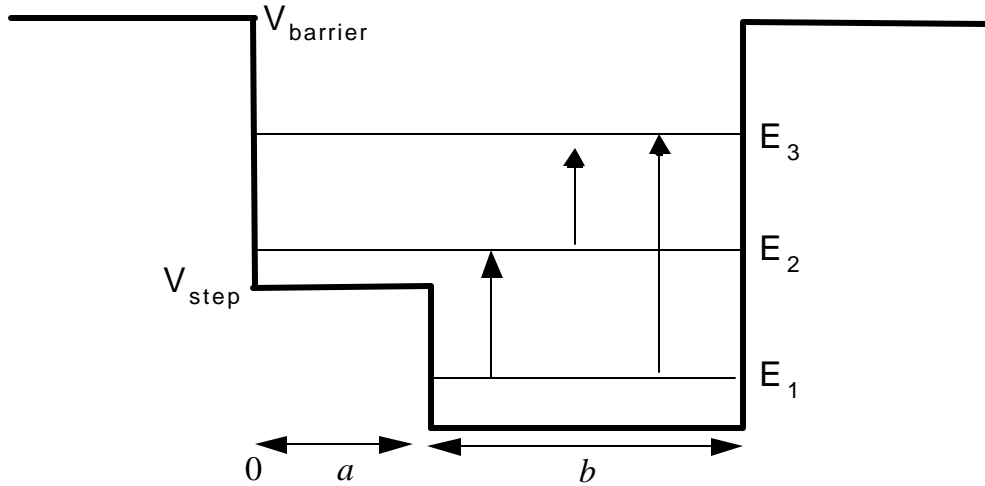
Figure 2.6   Asymmetric quantum well with allowed transitions.

In addition to allowing intersubband transitions between any low states, the asymmetric well structure also gives linear Stark shift (Yuh, 1989). This can be utilized for tuning the detection wavelength (Martinet , 1992).

E.   INTERSUBBAND ABSORPTION COEFFICIENT

The absorption coefficient in quantum well devices is one of the most important factor in the design of the quantum structures and is proportional to the amount of incident light that is absorbed in the structure. The absorption coefficient depends upon the material characteristics of the respective semiconductor. For example, the high refractive index of a semiconductor such as $GaAs$, (n = 3.3), causes that light incident on the surface of an epitaxial layer structure is refracted towards the normal, for example, and away from the required orientation. Efficient coupling of the intersubband transition can be achieved by a number of optical techniques, including the use of a beveled edged device (Levine, 1987), diffraction gratings (Hasnain, 1989), and combined diffraction gratings and waveguides (Andersson, 1992).

In addition to absorption, it is important to extract the photoexcited carriers out of the quantum well. This is achieved by placing the excited state near the top of the barrier as shown in Figure 2.7. In the case of the bound-to-continuum transition (see Figure 2.7a), the excited state is located just above the barriers, while for a bound-to-quasi

14

bound structure (see Figure 2.7b) the excited state is just below the barrier. The latter structure provides lower leakage current due to the higher barrier height for the same detection wavelength.
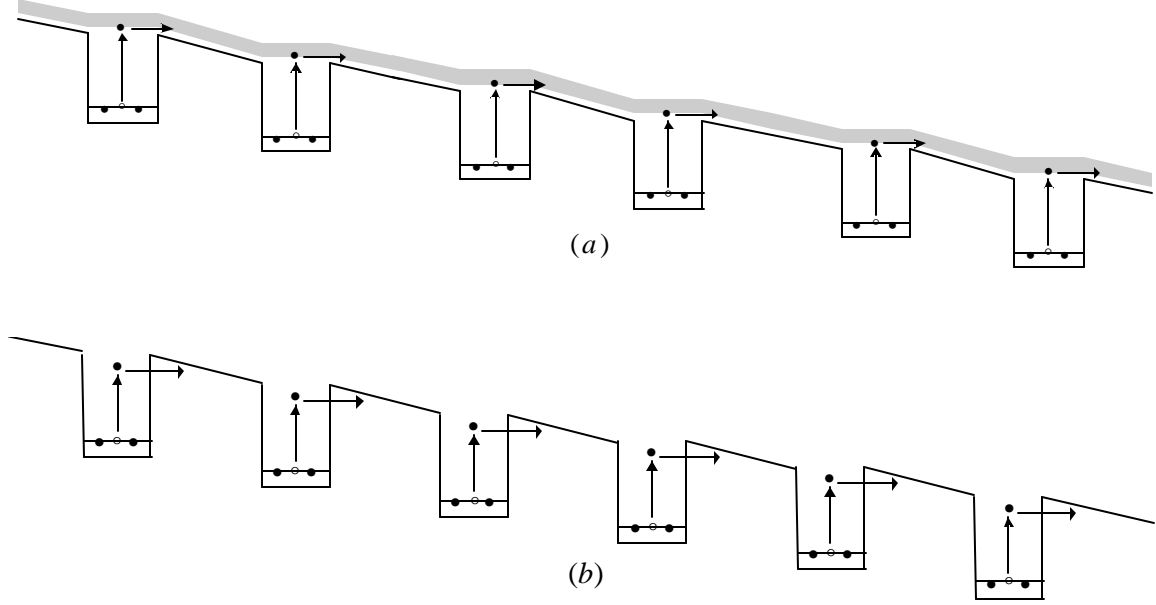
Figure 2.7   Bound-to-continuum (a) and (b) bound-to-bound transitions.

For the bound-to-bound transitions, since there is only one final state, the summation over the initial states in Equation 2.23 gives the number of the electrons in the ground state,

$$N = N_d LA.$$ (2.23)

Here, N is the number of electrons in the initial state, N_d is the three dimensional doping density, and L and A are the well width and area of the quantum structure, respectively. The delta function in Equation 2.15 is usually replaced by the normalized Lorentzian function to take into account the spectral line width given by (Yariv, 1997)

$$g(\hbar w) = \frac{1}{2p} \frac{\Gamma}{\left(E_f - E_i - \hbar w\right)^2 + \left(\Gamma/2\right)^2},$$ (2.24)

where Γ is the full width at half the maximum. This is usually obtained experimentally and is about 10-20 *meV* for intersubband absorption. The transition rate, found using the interaction potential and the momentum operator is given by

$$W_{Bound \to Bound} = \frac{N_d (IAL) e^2 \hbar^3}{(\hbar w)\left(m_e^*\right)^2 e_0 n_r c} |< y_f | \frac{d}{dz} | y_i >|^2 \, g(\hbar w).$$

(2.25)

For the bound-to-continuum transitions, the number of initial states is still N with energy E_i, as in the case of bound-to-bound states. However, the summation over the final states requires multiplication by the joint density of states $r(E)$, which is defined as

$$r(E)dE = \frac{2dk_z}{\left(\frac{2p}{l}\right)}.$$

(2.26)

For energy states separated by the incident photon energy, the above equation can be reduced to

$$r(E) = \frac{l}{2p} \sqrt{\frac{2m_b^*}{\hbar^2 (E_f - V_b)}}.$$

(2.27)

In this expression, l is the length of the region used for the normalization of the extended state wavefunction, m_b^* is the electron effective mass in the barrier, and V_b is the potential height of the barrier. The transition rate for bound-to-continuum states is then defined as

$$W_{Bound \to Continuum} = \frac{N_d (IAL) e^2 \hbar^2 l}{2\left(m_e^*\right)^2 e_0 n_r c} \sqrt{\frac{2m_b^*}{(\hbar w)^2 (E_f - V_b)}} |< y_f | \frac{d}{dz} | y_i >|^2.$$

(2.28)

This model of the bound to free intersubband absorption is one where the line width is due only to the variation of the joint density of states. The absorption coefficient $a(\hbar w)$ can be obtained by using both the transition of the matrix element and the transition rate as follows:

$$a(\hbar w) = \frac{\text{number of transitions per unit volume and time}}{\text{incident photon flux}}, \quad a(\hbar w) = \frac{W/AL}{I}.$$

(2.29)

Thus, the absorption coefficients for the bound-to-bound and bound-to-continuum transitions are given by

16

$$\boldsymbol{a}_{Bound \to Bound}(\hbar w) = \frac{N_d e^2 \hbar^3}{(\hbar w)\left(m_e^*\right)^2 \boldsymbol{e}_0 n_r c} |<\boldsymbol{y}_f| \frac{d}{dz} |\boldsymbol{y}_i>|^2 \, g(\hbar w)$$

<div align="right">(2.30)</div>

$$\boldsymbol{a}_{Bound \to Continuum}(\hbar w) = \frac{N_d e^2 \hbar^2 l}{2\left(m_e^*\right)^2 \boldsymbol{e}_0 n_r c} \sqrt{\frac{2m_b^*}{(\hbar w)^2 (E_f - V_b)}} |<\boldsymbol{y}_f| \frac{d}{dz} |\boldsymbol{y}_i>|^2 \, .$$

The length term, l, which appears in the bound-to-continuum transition, is eliminated by the $\frac{1}{l}$ term in the normalized final state wave function (assuming it is confined to a length, l). As an example, absorption coefficients for the bound-to-bound and bound-to-continuum situations for the quantum well shown in Figure 2.8 are depicted in Figures 2.9 and 2.10, respectively.
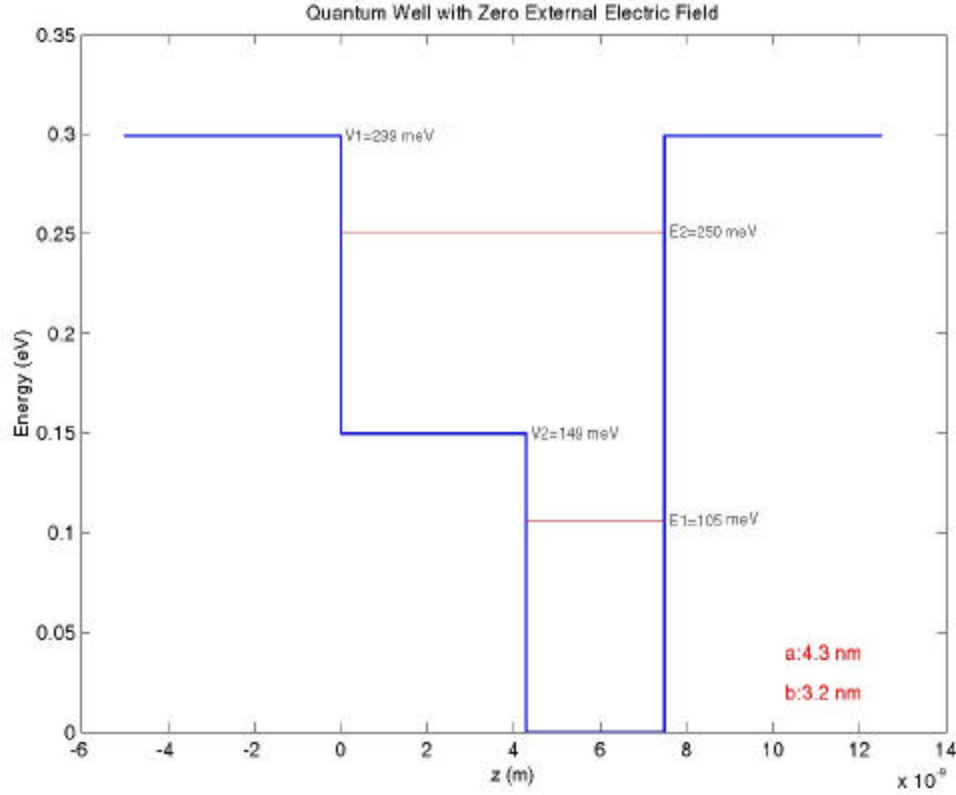
Figure 2.8   Energy levels of the $Al_{0.40}Ga_{0.60}As \, / \, Al_{0.20}Ga_{0.80}As \, / GaAs \, / \, Al_{0.40}Ga_{0.60}As$ quantum potential well.
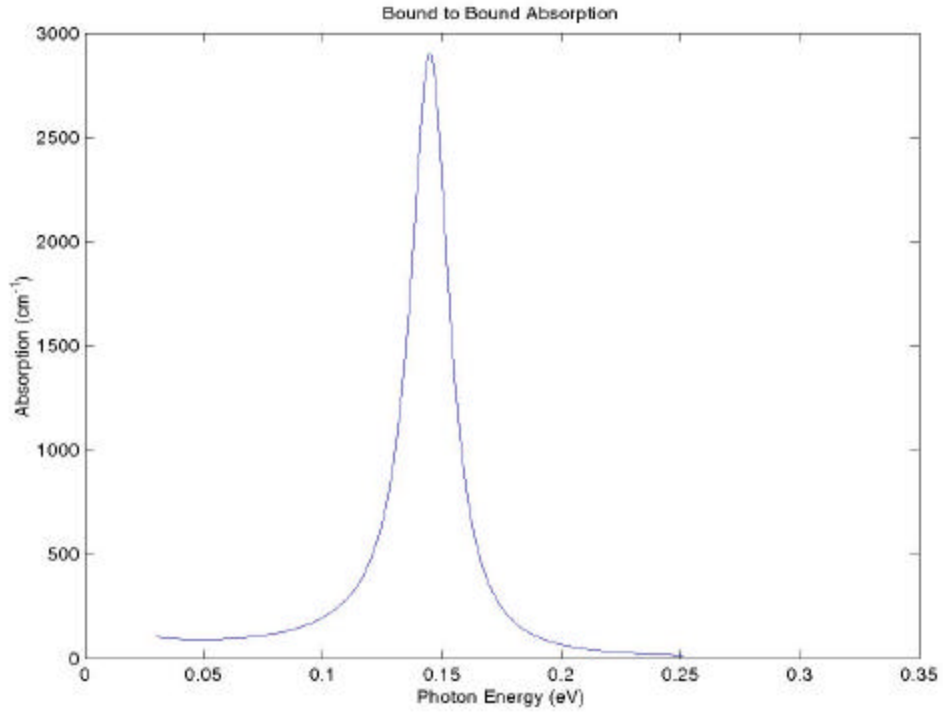
Figure 2.9   Bound-to-bound absorption coefficient for the quantum potential well
given in Figure 2.8 with $\Gamma = 20\ meV$.

Figure 2.9 shows the absorption versus photon energy for bound-to-bound transitions. There is a sharp rise in the absorption spectrum when the photon energy is equal to the difference between the bound state energies in the quantum well structure. The width of the curve depends on the finite lifetime of the excited electron, which was modeled using the Gaussian spectral density function.
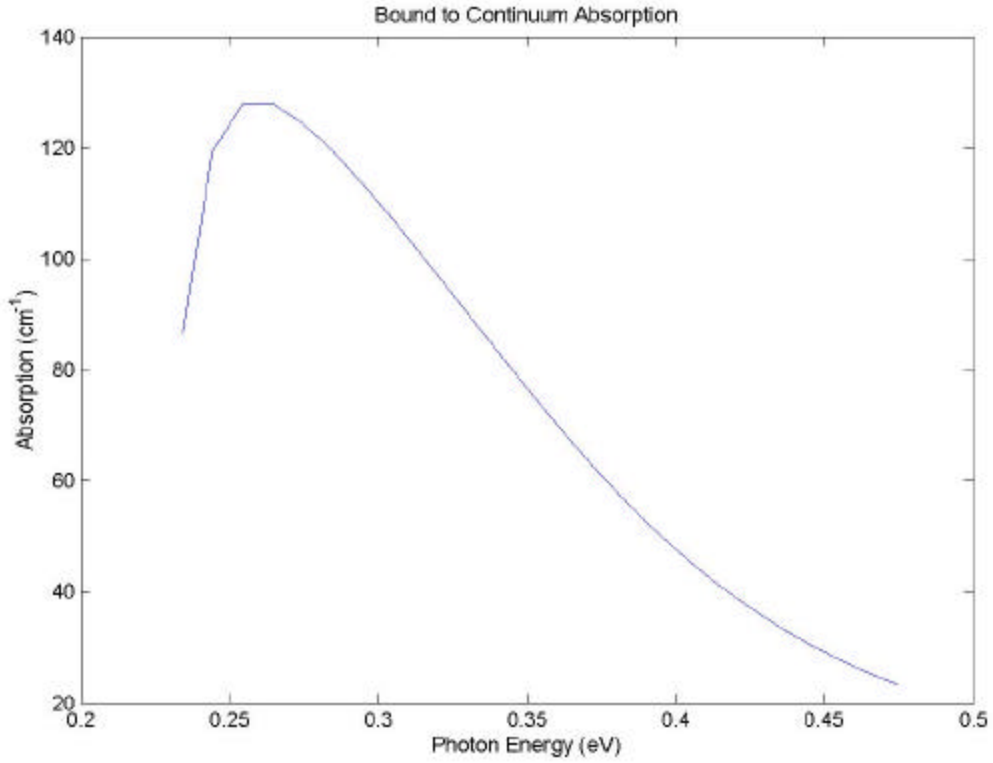
Figure 2.10   Bound-to-continuum absorption coefficient for the quantum well
in Figure 2.8.

Similarly, Figure 2.10 shows the absorption coefficient versus the photon energy for the case of bound-to-continuum transitions. The sharp rise in the spectrum corresponds to a photon energy equal to the difference between the bound state energy and the energy at the top of the quantum well where the extended continuum states begin. As the photon energy increases above this threshold value, absorption increases until reaching a peak value corresponding to the energy above the top of the barrier. At very high energies there is a slow decrease of $a(\hbar w)$ since the density of states drops as the energy is increased.

As previously mentioned, our goal is to design a detector with tunable bandwidth. The most convenient way to do this is by using bias as the tuning parameter. As a result, it is important to study the effect of bias on the energy levels as well as on the absorption.

F.   EFFECT OF ELECTRIC FIELD ON QUANTUM WELLS

When a uniform electric field is applied along the z direction (growth direction), the quantum well structure will tilt in the opposite direction of the electric field and the change due to this tilt will affect the energy states of the quantum well. The potential experienced by an electron in the quantum well is given by

$$V(z) = V_n + eFz,$$ (2.31)

where V_n is the potential height of the nth layer of the quantum well, e is the electron's charge, F, measured in (V/m), is the electric field strength , which is applied along the growth direction. A square quantum well in the presence of an external bias is shown in Figure 2.11.
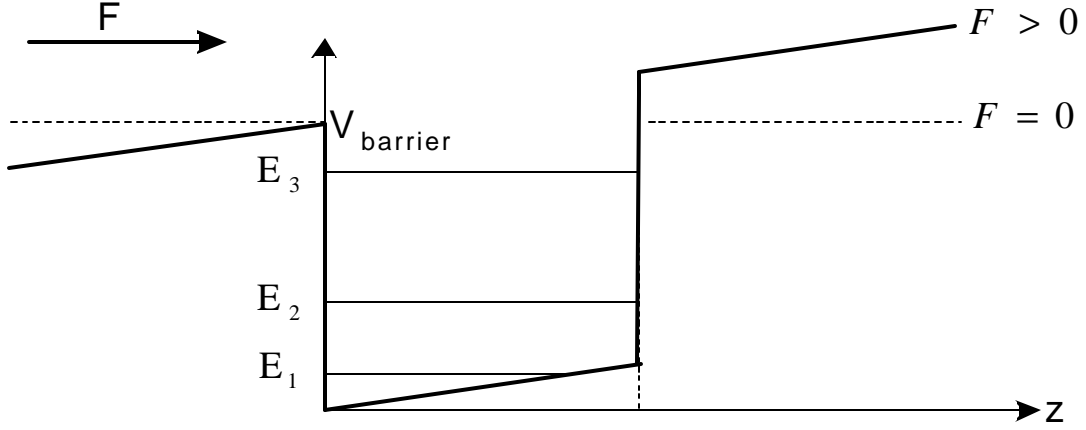
Figure 2.11   Schematic representation of a square quantum well under an applied bias.

By increasing the electric field, the lowest energy state E_1 in the quantum well will decrease in energy and fall into to the triangular potential formed at the bottom of the well. On the other hand, the excited states are less affected by the external electric field. However, for low electric field strengths, the shifting of all the energy levels are the same due to the symmetry of the square well. Thus, there is no appreciable Stark effect. This can be altered using an asymmetric quantum well, which is equivalent to a square well under a high electric field.

1.   Transfer Matrix Approach for Quantum Wells Under Applied Bias

Previously, we have discussed the calculation of the energy levels and wavefunctions of arbitrary quantum wells using transfer matrix approach. However, this approach cannot be used directly due to the linear variation of the potential energy under an external bias.

One way to overcome this problem is to approximate the linear potential due to the bias shown in Figure 2.12, with a series of steps or "staircase" as shown in Figure 2.13. The advantage of this approach compared to the use of Airy functions is that, it can be used at low field strengths, whereas Airy functions tend to diverge at low bias voltages, making the numerical analysis much more difficult (Brennan, 1987).
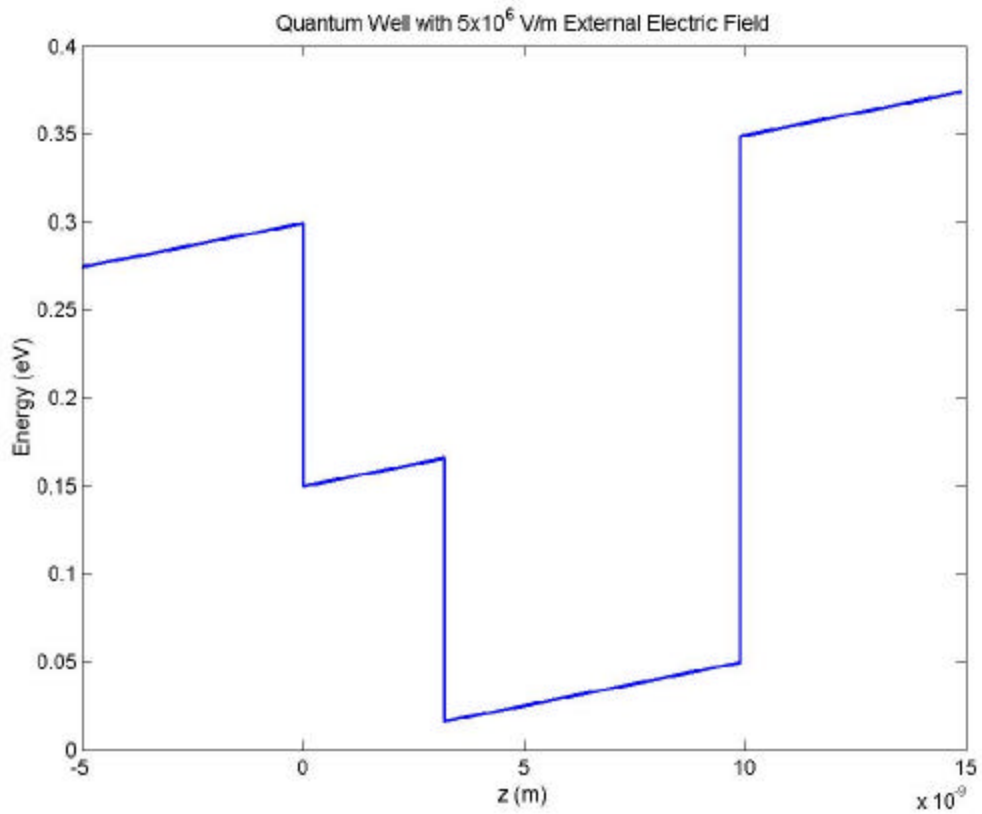
Figure 2.12   Step quantum well with applied bias of 5 V/mm.
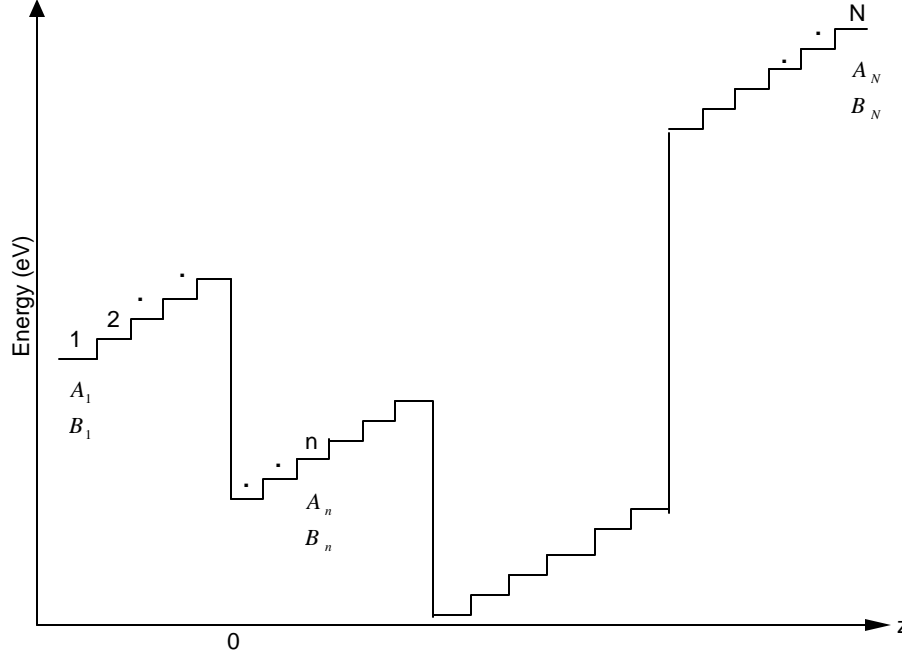
Figure 2.13   The stair case approximation of the potential shown in Figure 2.12.

The Schrödinger equation for an electron in the quantum well in the presence of an electric field F can be written as

$$-\frac{\hbar^2}{2m_n^*}\frac{d^2}{dz^2}\Psi_n - (E - V_n - qF z)\Psi_n = 0, \qquad (2.32)$$

where E is the energy of the electron in the layer and V_n and m_n^* are the potential and the effective mass in the nth layer, respectively. In order to apply the transfer matrix relations it is necessary to know the boundary conditions at the end points. For bound states, we can use the same approach as used in the zero bias case. For the continuum states we can assume that the electron is incident from the left side of the potential shown in Figure 2.13, and which gives $B_N = 0$. Thus, starting from $\begin{bmatrix} A_1 \\ B_1 \end{bmatrix}$, all the unknown $\begin{bmatrix} A_n \\ B_n \end{bmatrix}$ coefficients can be progressively calculated, ending with the coefficient $\begin{bmatrix} A_N \\ 0 \end{bmatrix}$. Therefore the electron wave functions can easily be obtained because all the coefficients are produced when A_1 is known (Hutchings, 1989).

Figures 2.14 (a) through 2.14 (d) show the potentials and eigenenergies calculated using the "staircase" approximation for external bias varied from 0 to $5V/mm$. In this way, we can observe the change in the energy states as a result of the applied electric field. Table 2.1 shows the change in bound state energies due to the external applied bias in the quantum well.

(a)

(b)

(c)

(d)
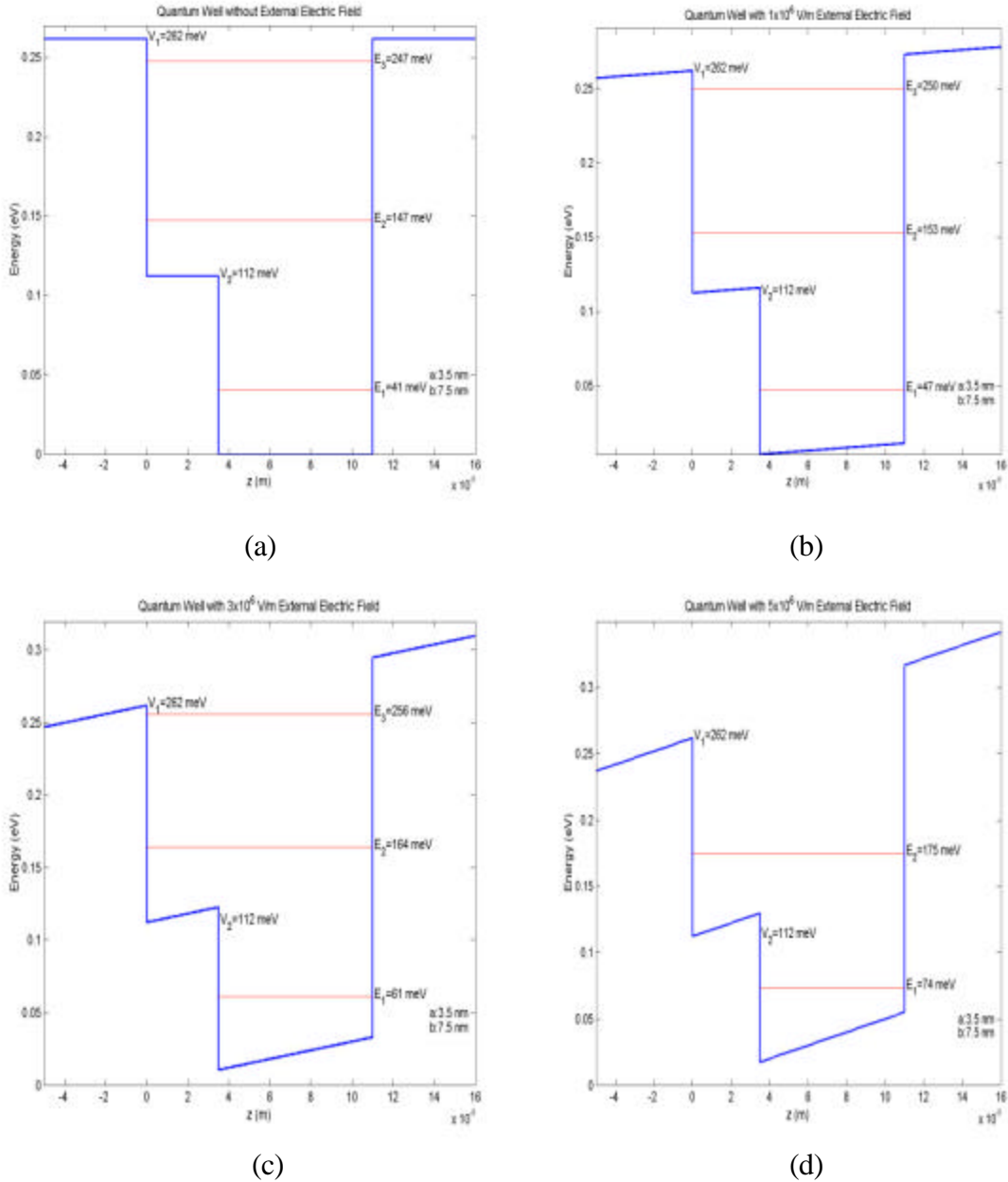
Figure 2.14   Effect of electric field on the bound state energies of a step quantum well for the following field strengths: (a) $F = 0$, (b) $F = 1$ V/mm, (c) $F = 3$ V/mm and (d) $F = 5$ V/mm.

Energy States	Zero Biased Well (meV)	$1V/mm$ Biased Well (meV)	$3V/mm$ Biased Well (meV)	$5V/mm$ Biased Well (meV)
E_1	41	47 ?E=6	61 ?E=20	74 ?E=33
E_2	147	153 ?E=6	164 ?E=17	175 ?E=28
E_3	247	250 ?E=3	256 ?E=9	-- Continuum

Table 2.1   Bound state energies as a function of bias.

2.   Intersubband Absorption Under an Applied Electric Field

The intersubband absorption peak position will shift in energy with changing electric field due to the shift of the energy levels. At a low bias, this effect is especially pronounced in asymmetric quantum wells as compared to symmetrical wells. Figure 2.15 shows the calculated absorption coefficient as a function of bias across the well using Equation 2.30. The matrix element in Equation 2.30 is evaluated using the wavefunction under the applied bias.
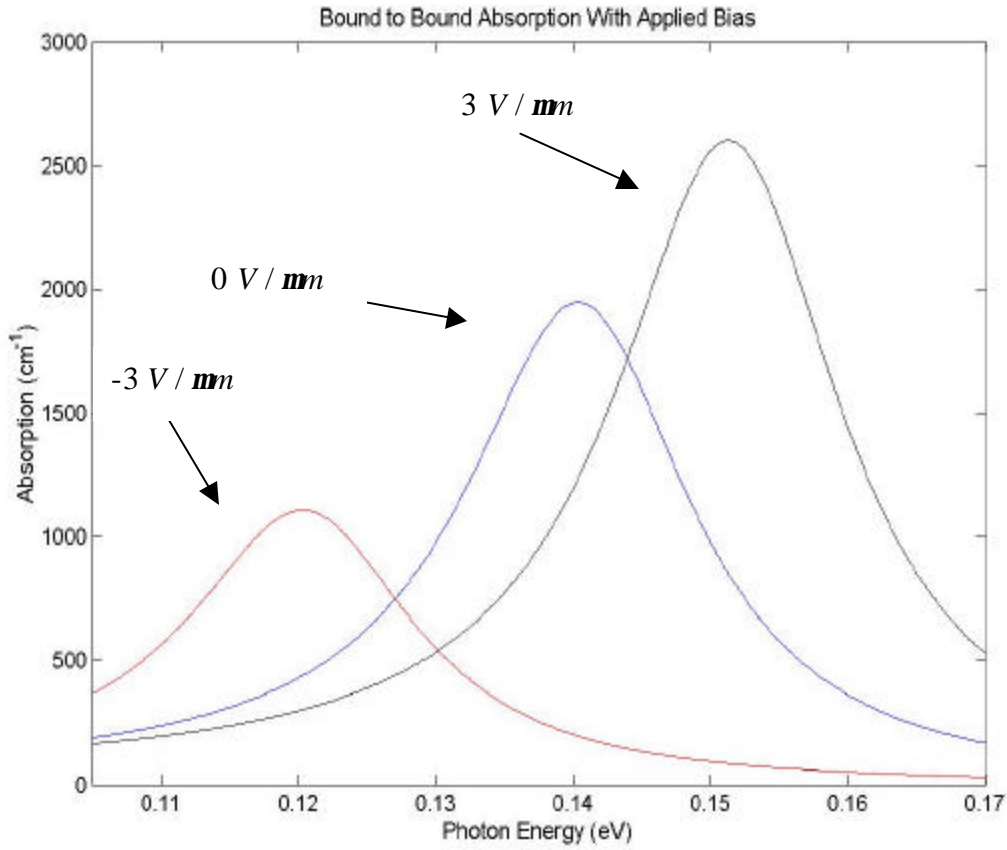
Figure 2.15   Absorption coefficient as a function of bias across the step quantum well structure.

The strength of absorption is found to increase with increasing electric field, mainly due to the stronger matrix element. The asymmetry observed between positive and negative biases is due to the fact that under forward bias (negative), the first excited energy level moves toward the ground state and hence the transition energy is reduced, while under reverse bias (positive) the opposite is true and the transition energy is increased.

G.   COMPARISON WITH EXPERIMENT

In order to verify the validity of the "staircase" model for a quantum well under bias, we have analyzed a step quantum well structure employed by Martinet *et al.*

(Martinet, 1992) for the study of bias dependent photocurrent. The parameters of the structure used in Martinet's experiment are shown in the Table 2.2.

Entered Experimental Data	
Layer and Thickness	Concentration
AlGaAs (barrier) 36.5 *nm*	0.40
AlGaAs (step) 6.7	0.20
GaAs 3.2 *nm*	--
AlGaAs (barrier) 36.5 *nm*	0.40

Table 2.2   Parameters of the step quantum well structure used by Martinet *et al.* (Martinet, 1992).

Figure 2.16 shows the step well structure and the calculated energy levels using the Matlab program developed using the "staircase" approximation for the same structure used by Martinet *et al.* (Martinet, 1992).
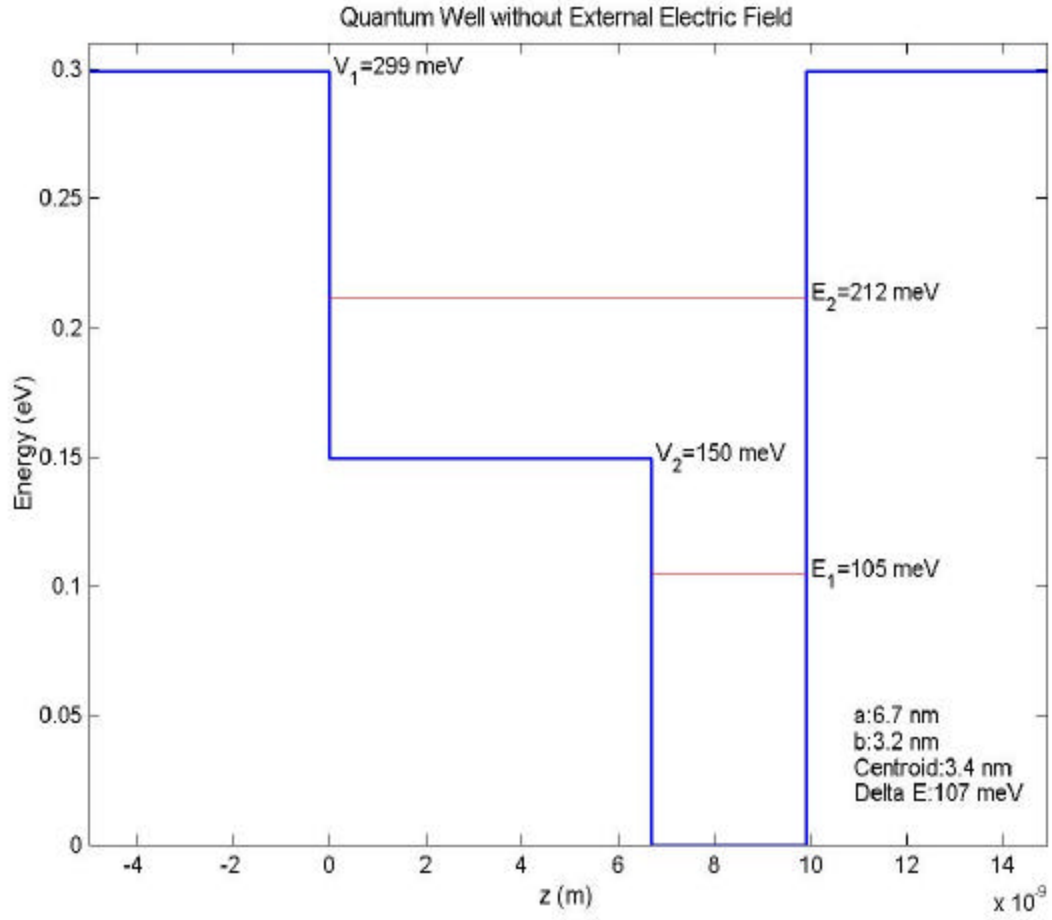
Figure 2.16   Calculated energy levels of the $Al_{0.40}Ga_{0.60}As / Al_{0.20}Ga_{0.80}As / GaAs$ step quantum well.

The calculated value of $E_2 - E_1$ of 107 *meV* is close to the zero-field absorption peak of 115 *meV* observed experimentally. The experimentally observed shift of the absorption peak (Martinet, 1992) for different electric fields in the step quantum well is shown in Figure 2.17.
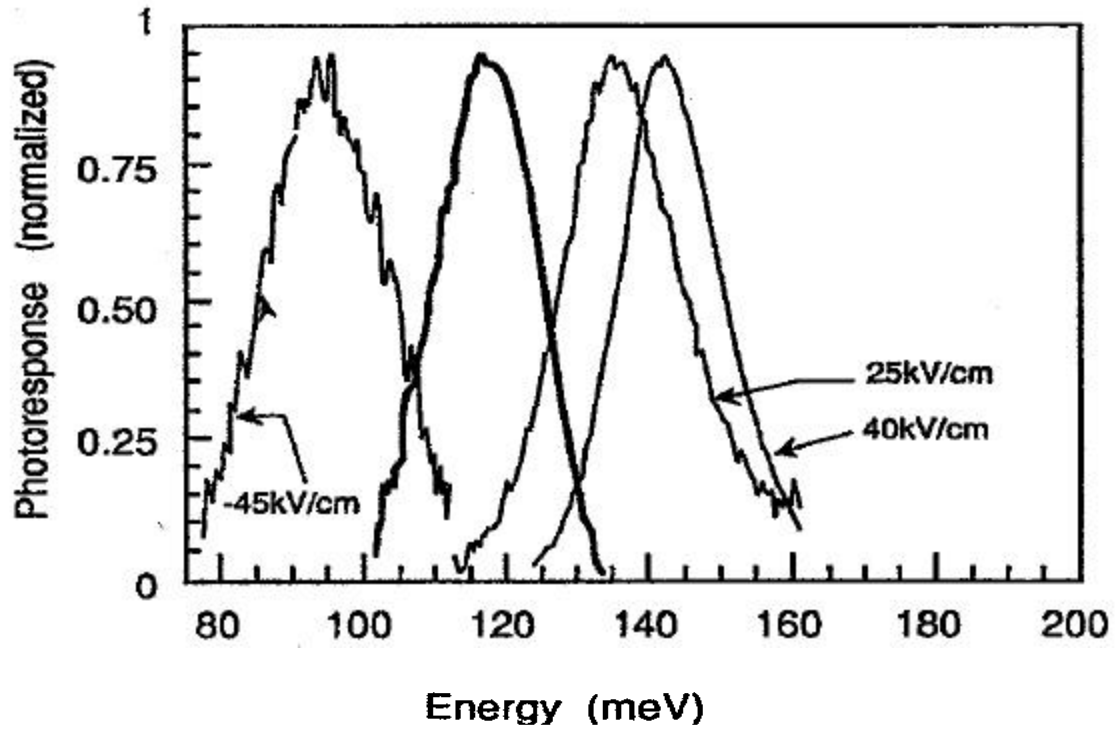
Figure 2.17   Normalized responsitivity of the asymmetric step quantum well under
different positive and negative biases. The peak shift is nearly four times the spectral
width. Zero field absorption (bold line) is included as a reference, (Martinet , 1992).
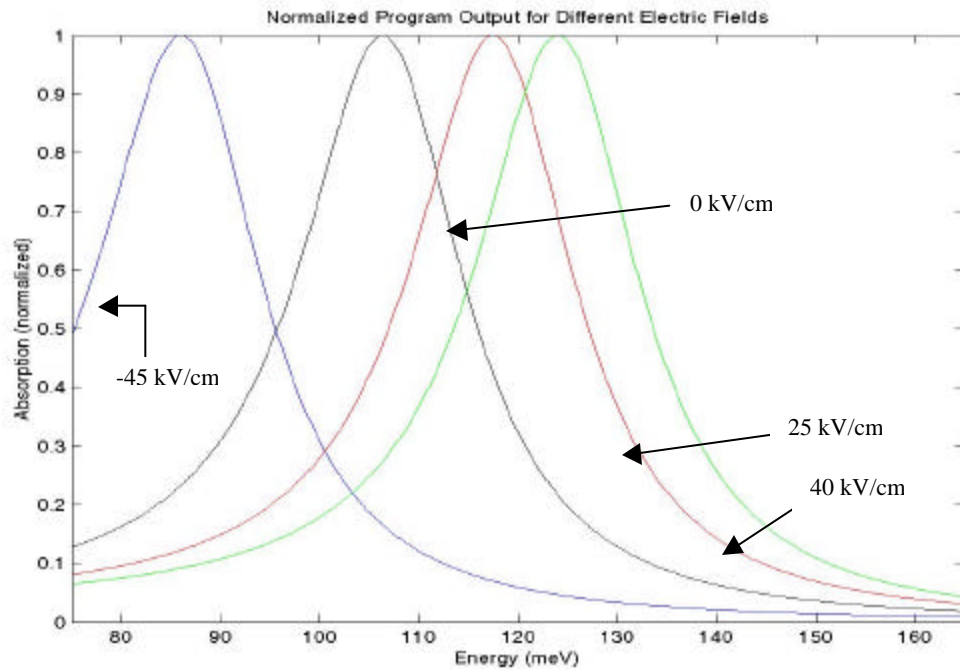
Figure 2.18   Plot of bound-to-bound, $1 \rightarrow 2$ normalized absorption transitions with
$\Gamma = 20\,meV$ done with the Matlab program.

28

Figure 2.18 shows the calculated absorption coefficient (normalized) for the same set of bias voltages as in the experiment. The experiment shows that the peak position changes from $93\ meV$ to $145\ meV$ when the bias is changed from $42\ kV/cm$ to $-40\ kV/cm$. The calculated value of the peak changes from $86\ meV$ to $125\ meV$ for the same bias values. The experimental and calculated peak shifts amount to $52\ meV$ and $39\ meV$, respectively. The difference between the two values may be due to the comparison of the photocurrent versus the absorption coefficient. Nonetheless, the results show that the model predictions are in reasonably good agreement with the experimental observation, indicating the accuracy of the calculation.

H.   SUMMARY

In this chapter the transfer matrix method was derived for an arbitrary potential well. This technique was employed to calculate the energy levels and wavefunctions of a step potential well. Intersubband transition selection rules in both symmetric and asymmetric potential wells and how they affect the design of the detector were also discussed. Another significant design parameter, the absorption coefficient, was calculated for both symmetric and asymmetric wells. External bias and its effects on the quantum wells, energy levels, and absorption coefficients were discussed. The use of "staircase" approach to calculate the absorption coefficient is found to be in good agreement with the experimental observation. In the following chapter, the design of the tunable bandwidth quantum well detector will be discussed.

THIS PAGE INTENTIONALLY LEFT BLANK

III. DESIGN OF A TUNABLE BANDWIDTH AlGaAs/GaAs STEP QUANTUM WELL INFRARED PHOTODETECTOR

A. INTRODUCTION

As discussed in Chapter II, intersubband absorption results from transitions between the energy levels of a quantum well formed within the conduction or valence band. This section presents detailed calculations of energy level, wavefunction and oscillator strength in an $AlGaAs/GaAs$ step well structure. The use of an electric field to tune the detection bandwidth will also be described. First, however, the calculations of effective mass and barrier height as a function of Al composition in the $Al_xGa_{1-x}As$ layer will be discussed.

B. EFFECTIVE MASS AND BARRIER HEIGHT CALCULATION

Normally the band offsets of the conduction band (ΔE_c) and valence band (ΔE_v) of $Al_xGa_{1-x}As/GaAs$ quantum well structures can be calculated by using the total band offset (ΔE_g). Accepted values of conduction and valence band offset ratios are as follows (Meyer, 2001):

$$\Delta E_c = 0.6\Delta E_g$$
$$\Delta E_v = 0.4\Delta E_g \ . \tag{3.1}$$

The bandgap of $Al_xGa_{1-x}As$, $E_g(x)$, can be approximately calculated using Vegard's Law as (Adachi, 1994)

$$E_g(x) = xE_{g(AlAs)} + (1-x)E_{g(GaAs)} \ , \tag{3.2}$$

where x is the Al molar fraction and $E_{g(AlAs)}$ and $E_{g(GaAs)}$ are the bandgaps of $AlAs$ and $GaAs$, respectively, at the $\Gamma-$ point.

Using the experimentally observed band gaps of $AlAs$ $(2.671\ eV)$ and $GaAs$ $(1.424\ eV)$, the band gap of $Al_xGa_{1-x}As$ at the $\Gamma-$ point is given by (Singh, 1993)

$$E_g(x) = 1.424 + 1.247x \quad eV \tag{3.3}$$

The graph in Figure 3.1 shows the band gap of the $Al_xGa_{1-x}As$ layer as a function of Al composition where the composition x changes from zero to one hundred percent.
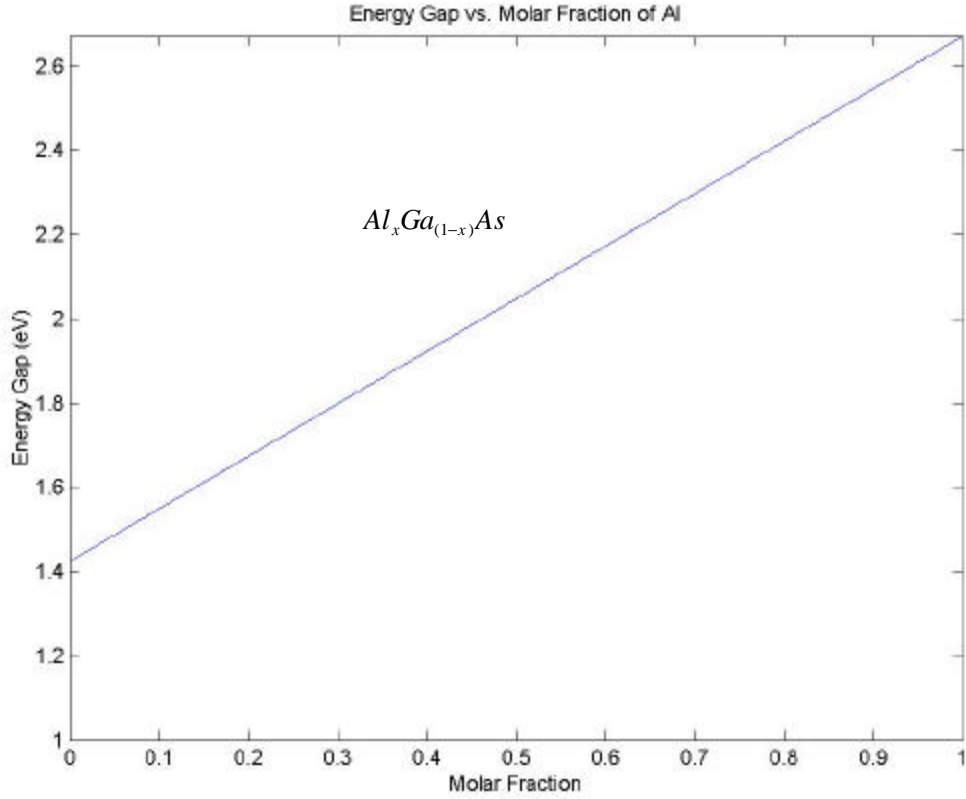
Figure 3.1   Energy gap at $\Gamma-$ point as a function of Al.

1.   Effective Mass Calculation

The effective mass of the $Al_xGa_{1-x}As$ alloy can also be found using Vegard's Law as

$$\frac{1}{m^*_{(AlGaAs)}} = \frac{x}{m^*_{(AlAs)}} + \frac{1-x}{m^*_{(GaAs)}}. \qquad (3.4)$$

The inverse relationship is due to the fact that the effective mass and energy are inversely related, where

$$m^*_{(AlAs)} = 0.15 m_e$$
$$m^*_{(GaAs)} = 0.067 m_e \qquad (3.5)$$

32

are the Γ point effective masses of *AlAs* and *GaAs*, respectively(Singh, 1993).

Figure 3.2 shows the plot of effective mass as a function of *Al* composition.
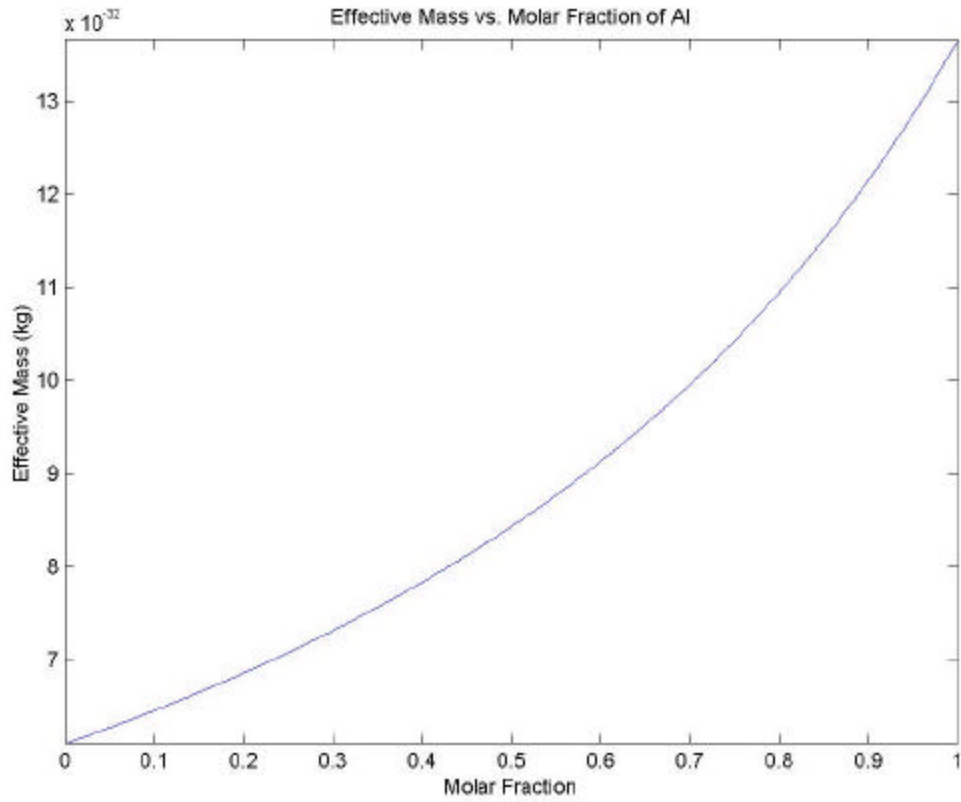
Figure 3.2   Effective mass vs. molar fraction of *Al*.

THIS PAGE INTENTIONALLY LEFT BLANK

IV. FINAL DESIGN OF THE STRUCTURE

In the following, we will discuss the design of a tunable bandwidth detector with center wavelength near 8.5 μm. The most convenient material system is $AlGaAs/GaAs$ due to their lattice match and to mature growth technology. In order to demonstrate the band tuning capability, a bound-to-bound transition in a step quantum well will be used. Figure 4.1 shows a step well with peak absorption near 8.9 μm. This structure was optimized to achieve a relatively large absorption coefficient with peak absorption between 8 and 9 μm. The first excited state lies about 24 meV below the barrier edge.
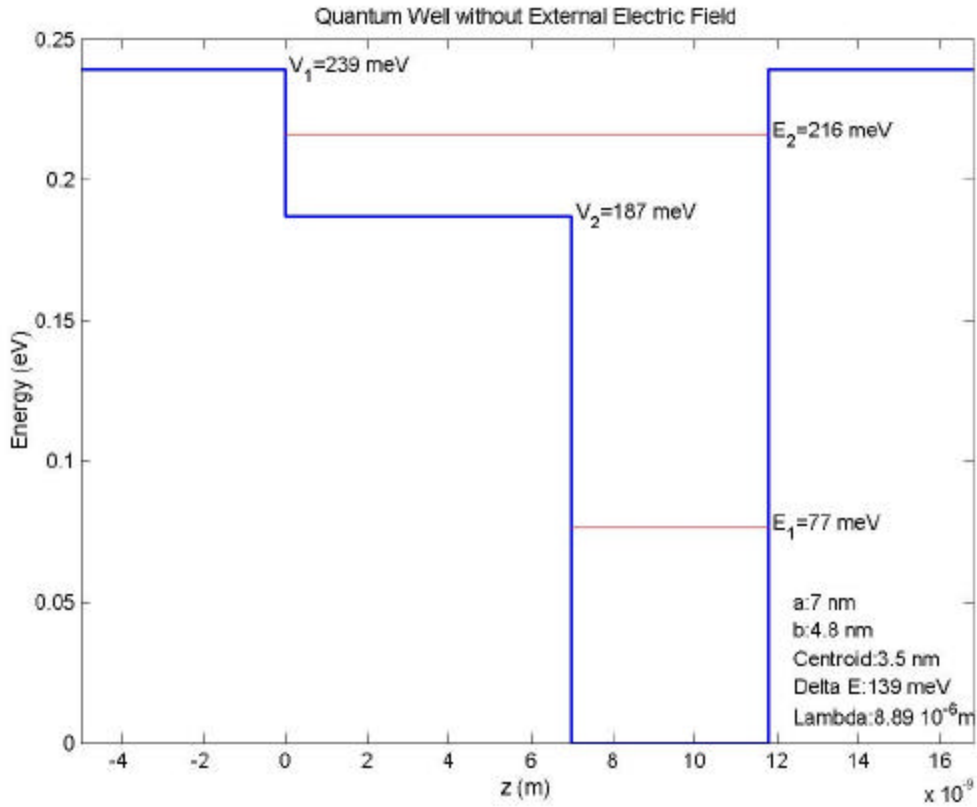
Figure 4.1   Optimized quantum well showing the energy levels, centroids, and lambda.

Figure 4.2 shows the calculated absorption coefficient of the structure for a set of positive and negative bias voltages.
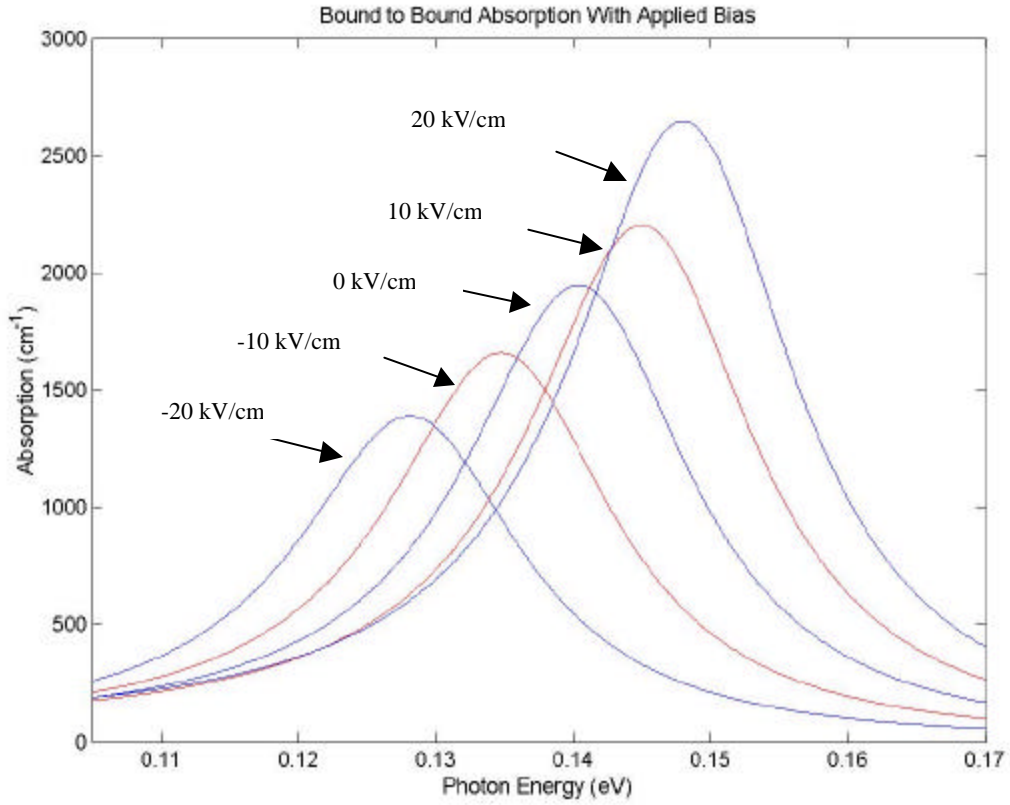
Figure 4.2   Absorption coefficient for bound-to-bound intersubband transition for the
step well shown in Figure 4.1 for a set of bias voltages.

Table 4.1 shows E_1, E_2, and oscillator strength, f, for the quantum well structure given

in Figure 4.1 under various applied biases.

Energy states and oscillator strength	Zero Biased Well	$1V/mm$		$2V/mm$		$3V/mm$	
		V	-V	V	-V	V	-V
$E_1(eV)$	0.0766	0.0833	0.0767	0.0926	0.0792	0.1017	0.0818
$E_2(eV)$	0.2160	0.2184	0.2220	0.2211	0.2275	0.2224	0.2334
f	0.1343	0.1146	0.1523	0.0960	0.1831	0.0766	0.1798

Table 4.1   Energy states and oscillator strengths under different biases for the
quantum well structure shown in Figure 4.1.

It can be seen in Figure 4.2 that the absorption peak shifts with applied bias due to the linear Stark effect in the step quantum well. However, the bandwidth of the absorption peak remains nearly the same. In order to achieve tunable bandwidth, a two step quantum well was arranged as shown in Figure 4.3.
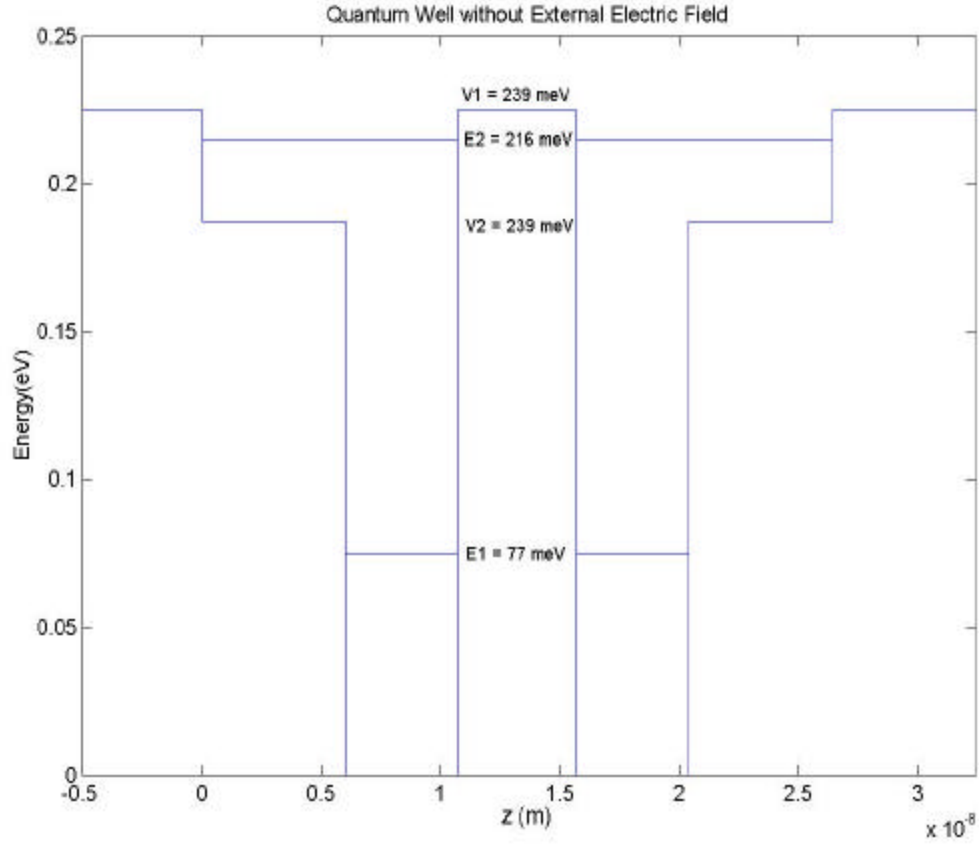
Figure 4.3   Final design of the asymmetric quantum well structure.

In this case, under a given bias the absorption peaks of the two wells move in opposite directions. Figure 4.4 shows the calculated absorption coefficient of the combined structure as a function of photon energy for a set of bias voltages.
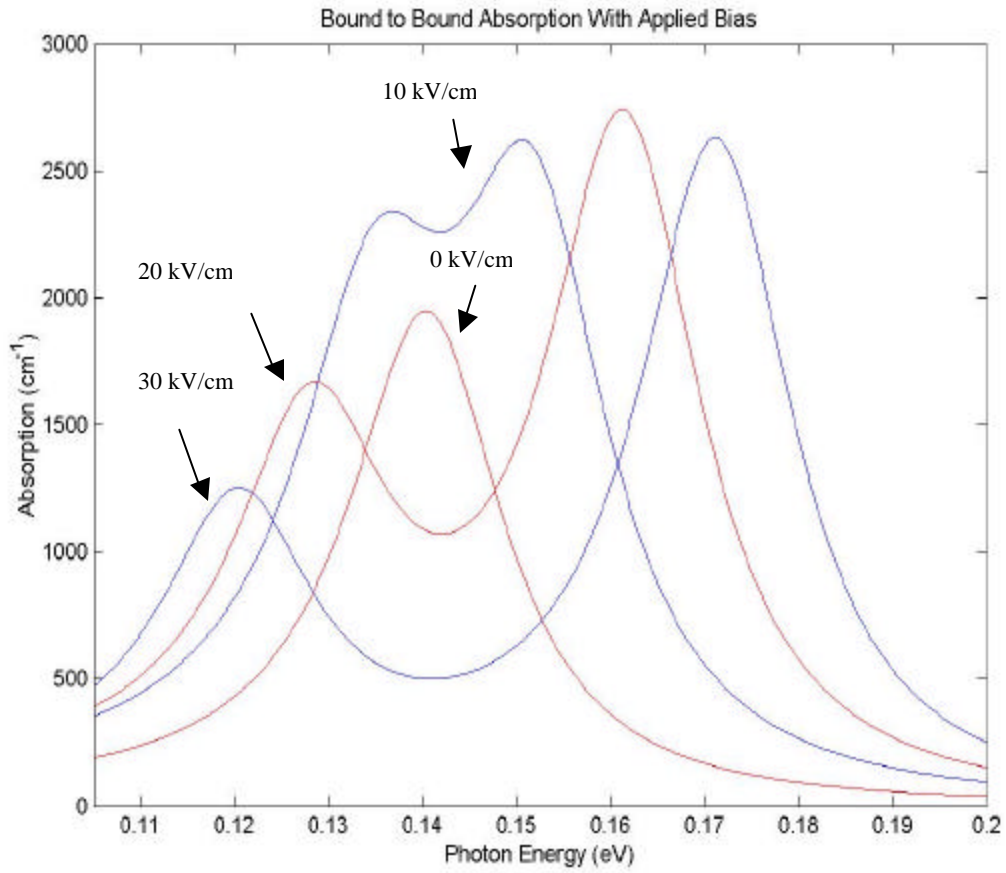
Figure 4.4   Calculated absorption coefficients for the combined step quantum well.

It can clearly be seen that the bandwidth increases as the bias increases. At 10 kV/cm, the bandwidth is nearly doubled. For higher electric fields, the absorption coefficient near the center drops due to a large shift of the two peaks. The details of the layer structure needed to fabricate the tunable bandwidth quantum well detector are shown in Table 4.2.

Layer and Thickness	Molar Fraction	Layer	m* (kg)	E_g (eV)
AlGaAs (barrier) 5 nm	0.32	$Al_{0.32}Ga_{0.68}As$	$0.0814m_0$	1.8230
AlGaAs (step) 7 nm	0.25	$Al_{0.25}Ga_{0.75}As$	$0.0778m_0$	1.7357
GaAs 4.8 nm	--	GaAs	$0.067m_0$	1.4240
AlGaAs (barrier) 5 nm	0.32	$Al_{0.32}Ga_{0.68}As$	$0.0814m_0$	1.8230
GaAs 4.8 nm	--	GaAs	$0.067m_0$	1.4240
AlGaAs (step) 7 nm	0.25	$Al_{0.25}Ga_{0.75}As$	$0.0778m_0$	1.7357
AlGaAs (barrier) 5 nm	0.32	$Al_{0.32}Ga_{0.68}As$	$0.0814m_0$	1.8230

Table 4.2   The layered structure of a tunable bandwidth step quantum well detector.

In summary, the design of a step quantum well structure for tunable bandwidth detection was introduced. The tunability of the detector by applying a bias to the quantum structure was also demonstrated.

THIS PAGE INTENTIONALLY LEFT BLANK

V.   CONCLUSION

The transfer matrix method was derived, and energy levels and wavefunctions for an asymmetric arbitrary potential well were calculated. Intersubband transition selection rules and their effect on the design process were also discussed. The absorption coefficient, which is also important in the design of a quantum well, was calculated for both symmetric and asymmetric wells. The "staircase" potential method was used to present both the effects of an external bias and the shift in the detection wavelength due to the various applied external electric fields across the detector. External bias and its effects on the quantum wells, energy levels, and absorption coefficients were explained in detail. The validity of the program was demonstrated through comparison with experimental data and the best possible design of the step quantum well structure for broadband detection was found.

A quantum well structure having a broadband detection capability was designed using two step quantum well structures arranged opposite to each other. This kind of structure allowed both blue and red Stark shifts of the transition energy producing a tunable bandwidth. The calculated absorption spectral bandwidth as a function of the applied bias shows that the peak width can be varied from $1.27 \ \mu m$ to $2.17 \ \mu m$, which is twice the bandwidth at zero bias.

Finally, the analysis indicates the possibility of fabricating a tunable bandwidth infrared detector using asymmetric quantum wells.

THIS PAGE INTENTIONALLY LEFT BLANK

APPENDIX. [SELECTED PROGRAMS]

```
%THIS PROGRAM FINDS BOUND ENERGY LEVELS IN ANY KIND OF STEP WELL
%by ATAKAN KONUKBAY © 2002
clear all,clc,close all;
global N x E1 h Ein v
N=input('Enter the number layers> '); %ENTER 1 FOR SQUARE,2 FOR STEP QUANTUM WELL

e=1.602e-19; %Coulomb
h=197.33e-9; %Planck's Constant

%MOLAR RATIOS (ENTER VALUES AS .35)
XX(1)=input('Enter the percentage of Al in region   I >');
XX(2)=input('Enter the percentage of Al in region  II >');
XX(3)=input('Enter the percentage of Al in region  IV >');

%THE ENERGY GAP IN EACH REGION OF THE ASYMMETRIC QUANTUM WELL
Eg1=1.424+1.247*XX(1);   %AlxGa(1-x)As
Eg2=1.424+1.247*XX(2);   %AlxGa(1-x)As
Eg3=1.424;               %GaAs
Eg4=1.424+1.247*XX(1);   %AlxGa(1-x)As

%EFFECTIVE MASSES
M=.511e6;
m(1)=1/((XX(1)/(0.15*M))+((1-XX(1))/(0.067*M)));
m(2)=1/((XX(2)/(0.15*M))+((1-XX(2))/(0.067*M)));
m(3)=0.067*M;
m(4)=1/((XX(3)/(0.15*M))+((1-XX(3))/(0.067*M)));

%POTENTIAL IN CONDUCTION BAND
v(1)=0.6*(Eg1-Eg3);
v(2)=0.6*(Eg2-Eg3);      %Set origin @ 0
v(3)=0;                  %.6*(Eg3-Eg2);
v(4)=0.6*(Eg1-Eg3);
%******

a=input('Enter the width from 0->a in Angstrom> ');
b=input('Enter the width from a->b in Angstrom> ');

x=[0 a a+b]*1e-10;

%******

E=0.0001;
Ein=input('Enter the energy  (eV)> ');
Efin=input('Enter the external E field (1e6 V/m)> '); %ENTER AS 1,2…ETC.
El_=Ein*1e4;
   while E<=Ein;
     for d=1:El_
        T=1;
        for n = 1:N+1
        k(n)=sqrt((2*m(n))*(E-v(n))/((h^2)));
        k(n+1)=sqrt((2*m(n+1))*(E-v(n+1))/((h^2)));
```

43

```
A(n)=(exp(i*(x(n)*(k(n)-k(n+1)))))*((k(n+1)*(m(n)))+(k(n))*(m(n+1)))/(2*(k(n+1))*(m(n)));
B(n)=(exp(-(i*(x(n)*(k(n+1)+k(n))))))*((k(n+1)*(m(n)))-(k(n))*(m(n+1)))/(2*(k(n+1))*(m(n)));
C(n)=(exp(i*(x(n)*(k(n)+k(n+1)))))*((k(n+1)*(m(n)))-(k(n))*(m(n+1)))/(2*(k(n+1))*(m(n)));
D(n)=(exp(-(i*(x(n)*(k(n)-k(n+1))))))*((k(n+1)*(m(n)))+(k(n))*(m(n+1)))/(2*(k(n+1))*(m(n)));

MM(n)={[A(n) B(n);C(n) D(n)]};
end

ZZ=1; %Unit matrix
  for n=1:N+1;
    ZZ=MM{n}*ZZ;
  end
M22=real(ZZ(2,2));

TT(d)={[T*M22,E]};

Tt(d,:)=TT{d};
E=E+.0001;
  end
end

zz=1;
 for z=1:El_-1
tt1(z)=Tt(z,1);
tt2(z+1)=Tt(z+1,1);
ttm=tt1(z)*tt2(z+1);
    if ttm<0
    E(zz)=[Tt(z,2)];
    zz=zz+1;

  end
end

end
clc
MLDRAWFINE

*************

%MLDRAWFINE
%THIS PROGRAM DRAWS THE SHAPE OF THE QUANTUM WELL & DIVIDES THE WIDTH OF
THE STRUCTURE INTO MANY STEPS
%by ATAKAN KONUKBAY © 2002

clc;
e=1.602e-19;%Coulomb
Edp=Efin;   %Bias
delta=1e-10;

X{1,1}=(x(1)-50e-10):delta:x(1);
for n=2:N+1
X{1,n}=x(n-1):delta:x(n);
end
X{1,n+1}=x(1,n):delta:(x(1,n)+50e-10);

for n=1:N+2
```

```matlab
  XL(1,n)=length(X{1,n});
  Y{1,n}=(Edp*X{1,n})*1e6;%cnst;
  YL(1,n)=length(Y{1,n});
end

 for n=1:N+2
   lgth=length(Y{n});
   Y_{1,n}=[Y{1,n}(1:lgth)]+v(n);

 end


x_=[];
y__=[];
for n=1:N+2
   x_=union(x_,X{n});
   y__=cat(2,y__,Y_{n});

end

for n=1:N+2
 hold on;
 plot(X{1,n},(Y{1,n}+v(1,n)));
end


for n=2:N+2
  LXf=XL(1,n);
  LYf=YL(1,n);
hold on
 line([X{n-1}(1,XL(1,n-1)),X{n-1}(1,XL(1,n-1))],[Y{n-1}(1,YL(1,n-1))+v(n-1),Y{n}(1,1)+v(n)])
 hold on
end

for n=1:length(E)
   switch N
   case 1
   hold on
 line([x(1),x(2)],[E(n),E(n)],'Color','r')
 hold on
case 2
 if E(n)<v(2)
   hold on
 line([x(2),x(3)],[E(n),E(n)],'Color','r')
 hold on
else
 line([x(1),x(3)],[E(n),E(n)],'Color','r')
end
end
end
 title(sprintf('Quantum Well With External Electric Field  %g 10^6 V/m',Efin));

 for n=1:N+2
  QA{n}=Y{n}+v(n);
  L(n)=length(QA{n});
end
```

```
switch N

        case 1

  AQ=QA{2};
  AQ(1)=[];
  AQ((L(2)-1))=[];
  QA{2}=AQ;
  v_=[];
case 2
  AQ=QA{2};
  AQ(1)=[];
  QA{2}=AQ;
  AQ=QA{3};
  AQ(1)=[];
  QA{3}=AQ;
  v_=[];
end
for n=1:N+2;
    v_=cat(2,v_,QA{n});
  end
  L=length(v_);
  v1=v(1);

xlabel(sprintf('a = %g nm , b = %g nm',x(2)*1e9,(x(3)-x(2))*1e9));
ylabel(sprintf('Energy (eV)',Efin));
set(findobj(gca,'Type','line','Color',[0 0 1]),...
   'Color','blue',...
   'LineWidth',1)
text(x(3)+28e-10,0+.01,sprintf('%g / %g / %g',XX(1),XX(2),XX(3)),...
   'HorizontalAlignment','left','FontSize',8)
for n=1:length(E)
text(x(3)+1e-10,E(n),sprintf('E%g=%g ev',n,E(n)),...
   'HorizontalAlignment','left','FontSize',8)
end
grid off;

**************

%THIS PROGRAM CALCULATES THE ENERGY LEVELS FOR MULTI STEP WELL
%by ATAKAN KONUKBAY © 2002

global N v x E1 h Ein
N=length(x_)-1;


e=1.602e-19; %Coulomb
h=197.33e-9; %Planck's constant

x=x_;
%******mass
m_1(1:XL(1))=m(1);
m_2(1:(XL(2)-1))=m(2);
m_3(1:(XL(3)-1))=m(3);
m_4(1:(XL(4)))=m(4);
mm=[m_1 m_2 m_3 m_4];
```

46

```
%******
v=v_;

E=0.0001;
Edrw=0;
Ein=input('Enter the energy level (eV)> ');
Efin=0
El_=Ein*1e4;
   while E<=Ein;
      for d=1:El_
         T=1;
         for n = 1:N+1
         k(n)=sqrt((2*mm(n))*(E-v(n))/((h^2)));
         k(n+1)=sqrt((2*mm(n+1))*(E-v(n+1))/((h^2)));

         A(n)=(exp(i*(x(n)*(k(n)-k(n+1)))))*((k(n+1)*(mm(n)))+(k(n))*(mm(n+1)))/(2*(k(n+1))*(mm(n)));
         B(n)=(exp(-(i*(x(n)*(k(n+1)+k(n))))))*((k(n+1)*(mm(n)))-
(k(n))*(mm(n+1)))/(2*(k(n+1))*(mm(n)));
         C(n)=(exp(i*(x(n)*(k(n)+k(n+1)))))*((k(n+1)*(mm(n)))-(k(n))*(mm(n+1)))/(2*(k(n+1))*(mm(n)));
         D(n)=(exp(-(i*(x(n)*(k(n)-
k(n+1))))))*((k(n+1)*(mm(n)))+(k(n))*(mm(n+1)))/(2*(k(n+1))*(mm(n)));

         MM(n)={[A(n) B(n);C(n) D(n)]};
         end

         ZZ=1; %Unit matrix
            for n=1:N+1;
               ZZ=MM{n}*ZZ;
            end
          M22=real(ZZ(2,2));

          TT(d)={[T*M22,E]};
         Tt(d,:)=TT{d};
         E=E+.0001;
      end
   end

   zz=1;

   for z=1:El_-1
   tt1(z)=Tt(z,1);
   tt2(z+1)=Tt(z+1,1);
   ttm=tt1(z)*tt2(z+1);
         if  ttm<0
         E(zz)=[Tt(z,2)];
         Edrw(zz)=E(zz)+.001;

         zz=zz+1;

      end
   end

end

**************
```

```
%THIS PROGRAM CALCULATES THE ALPHA FOR BOUND TO CONTINUUM TRANSITIONS
%by ATAKAN KONUKBAY © 2002

clc,close
e=1.602e-19;            %C
Nd=1e18/1e-6;           %1/m3
hbar=1.055e-34;         %J.s
EoE=8.85e-12*sqrt(13);  %F/m
c=3e8                   %m/s

ENG=v(1)+.0001:.0001:v(1)+.02;%-(E(2)-E(1)):.001:2*((E(2)-E(1)));

Alpha=Nd*e^2*hbar^2*sqrt((2*m(1)*9.11e-31/.511e6)./((((ENG-E(1)).*e).^2).*((ENG-
v(1)).*e)))./(2*((m(3)*9.11e-31/.511e6)^2)*EoE*c)*AvXRegBC.^2

plot(ENG,Alpha/1e2)
grid on
xlabel('h\prime\omega [eV]')
ylabel('Absorption [cm^{-1}]')
title('Bound to Continuum Absorption')

**************

%THIS PROGRAM CALCULATES THE ALPHA FOR BOUND TO BOUND TRANSITIONS
%by ATAKAN KONUKBA Y © 2002

clc,close
Nd=1e18/1e-6 %1/m3
e=1.602e-19; %C
hbar=1.055e-34 %J.s
T=20e-3*e/2 %J
EoE=8.85e-12*sqrt(13); %F/m
c=3e8 %m/s

HW=E(1)+.0001:.0001:E(2);
G=T./((((E(2)-E(1)-HW)*e).^2)+((T)^2));
CB_B=(Nd*(e^2)*(hbar^3))/(((m(3)*9.11e-31/.511e6)^2)*EoE*c);

Alpha=(CB_B.*G.*AvXRegMB_B^2)./(HW.*e)

plot(HW,Alpha/1e2)
grid on
xlabel('h\prime\omega [eV]')
ylabel('Absorption [cm^{-1}]')
title('Bound to Bound Absorption')

**************

%THIS PROGRAM CALCULATES THE WAVEFUNCTION FOR MULTISTEP WELL
%by ATAKAN KONUKBAY © 2002

clc;
figure;
delta=1e-10;

trans=MM;
```

48

```
trs=MM;
for n=2:N+1
   trans{1,n}=trs{1,n}*trans{1,n-1};
end

A(1,1)=0;
B(1,1)=1;
for n=1:N+1
wavtrans=trans{1,n};
A(1,n+1)=wavtrans(1,2)*B(1,1);
B(1,n+1)=wavtrans(2,2)*B(1,1);
end
A(1,1)=0;
B(1,1)=1;
B(1,(XL(1)+XL(2)+XL(3))-1:n+1)=0;

X{1,1}=-x(2):delta:x(1);
for n=2:N+1
X{1,n}=x(n-1):delta:x(n);
end
X{1,n+1}=x(1,n):delta:(x(1,n)+(x(1,n)-x(1,n-1)));

TotalIntegral=0;
for n=1:N+2
W{1,n}=A(1,n)*exp(i*k(1,n)*X{1,n})+B(1,n)*exp(-(i*k(1,n)*X{1,n}));

%%%***for the wave used in calculating the oscillation with -B parameter
W_BC{1,n}=A(1,n)*exp(i*k(1,n)*X{1,n})-B(1,n)*exp(-(i*k(1,n)*X{1,n}));
%%%***

W_{1,n}=conj(W{1,n});
integr{1,n}=(W{1,n}.*W_{1,n})*delta;
integregn{1,n}=sum(integr{1,n});
TotalIntegral=integregn{1,n}+TotalIntegral;
end

b1 = 1/(sqrt(TotalIntegral));
normwave=0;
for n=1:N+2;
WavReal{1,n}=b1*W{1,n};

%%%***Now multiplying with normalization factor to get the wave
WavRealBC{1,n}=b1*W_BC{1,n};
%%%***

WR_{1,n}=conj(WavReal{1,n});
Integ{1,n}=(WavReal{1,n}.*WR_{1,n})*delta;
Integral{1,n}=sum(Integ{1,n});
normwave=Integral{1,n}+normwave;
end
for n=1:N+2
 hold on;
 plot(X{1,n},WavReal{1,n});
 hold on;
end
*************
```

THIS PAGE INTENTIONALLY LEFT BLANK

LIST OF REFERENCES

Adachi, S., *GaAs and Related Materials*, pp. 237-238, World Scientific, 1994

Andersson, T. G. and W. Chen, "Intersubband transitions for differently shaped quantum wells under an applied electric field", *Appl. Phys. Lett.*, **60**, pp. 1591-1593, 1992

Brennan K. F. and C. J. Summers, "Transfer matrix approach to the analysis of an arbitraray quantum well structure in an electric field", *Appl. Phys. Lett.*, **55**, pp. 1082-1084, 1989.

Choi, K.K., *The Physics of Quantum Well Infrared Photodetectors*, pp. 131-133, World Scientific, 1997

Coon, D.D. and R.P.G. Karunasiri, "New mode of IR detection using quantum wells", *Appl. Phys. Lett.*, **45**, pp.649-651, 1984.

Coon, D.D. and R.P.G. Karunasiri and L.Z. Liu, "Narrow band infrared detection in multiquantum well structures", *Appl. Phys. Lett.*, **47**, pp.289-291, 1985.

Esaki, L. and R. Tsu, *IBM Research Note*, RC-2418, 1969.

Hasnain, G., B.F. Levine, D.L. Sivco and A.Y. Cho, "Mid-infrared detectors in the 3-5 µm band using bound to continuum state absorption in InGaAs/InAlAs multiquantum well structures", *Appl. Phys. Lett.*, **56**, pp. 770-772, 1989.

Hutchings, D. C., "Transfer matrix approach to the analysis of an arbitrary quantum well structure in an electric field", *Appl. Phys. Lett.*, **55**, pp. 1082-1084, 1989.

Gravé, I., A. Shakouri, N. Kruze and A. Yariv, "Voltage-controlled tunable GaAs/AlGaAs multistack quantum well infrared detector", *Appl. Phys. Lett.*, **60**, pp. 2362-2364, 1992.

Gunapala, S.D., J.K. Liu, M. Sundaram, S.V. Bandara, C.A. Shott, T. Hoelter, P.D. Maker and R.E. Muller, "Long Wavelength Quantum Well Infrared Photodetector (QWIP) Research at Jet Propulsion Laboratory", *Proc. SPIE*, **2744**, pp. 722-730, 1996.

Levine, B.F. K.K. Choi, C.G. Bethea, J. Walker and R.J. Malik, "New 10 µm infrared detector using intersubband absorption in resonant tunneling GaAlAs superlattices", *Appl. Phys. Lett.*, **50**, pp. 1092-1094, 1987.

Levine, B. F., C. G. Bethea, K. K. Choi, J. Walker, and R. J. Malik, "Bound-to-extended state absorption GaAs superlattice transport infrared detectors", *Jour. Appl. Phys.*, **64**, pp. 1591-1593, 1988.

Levine, B.F., A. Zussman, S.D. Gunapala, M.T. Asom, J.M. Kuo and W.S. Hobson, "Photoexcited escape probability, optical gain, and noise in quantum well infrared photodetectors", *Jour. Appl. Phys.*, **72**, pp. 4429-4443, 1991.

Levine B. F. "Quantum-well infrared photodetectors", *Jour. Appl. Phys.*, **74**, pp. R1-R81, 1993.

Meyer, J. R. and Vurguftman I., "Band parameters for III-IV compound semiconductors and their alloys", *Jour. Appl. Phys.*, **89**, pp. 5855-5856, 2001.

Martinet, E., F. Luc, E. Rosencher, Ph. Bois, and S. Delaitre, "Electrical tunability of infrared detectors using compositionally asymmetric GaAs/AlGaAs multiquantum wells", *Appl. Phys.*, **60**, pp. 92-60, 1992.

Mii, Y. J, R. P. G. Karunasiri, K. L. Wang, M. Chen, and P. F. Yuh, "Bound-to-extended state absorption GaAs superlattice transport infrared detectors", *Jour. Appl. Phys.*, **64**, pp. 1591-1593, 1988.

Mii, Y. J., K. L. Wang, R. P. G. Karunasiri, and P. F. Yuh, "Observation of large oscillator strengths for both $1 \rightarrow 2$ and $1 \rightarrow 3$ intersubband transitions of step quantum wells", *Appl. Phys. Lett.*, **56**, pp. 1046-1048, 1990.

Robinett, Richard W., *Quantum Mechanics*, pp. 115, Oxford University Press, 1997

Singh, J., *Physics of Semiconductors and Their Heterostructures*, pp. 184-185, McGraw-Hill Book Co., 1993.

Smith, J.S., L.C. Chiu, S Margalit, A. Yariv and A.Y Cho, "A new infrared detector using electron emission from multiple quantum wells", *J. Vac. Sci. Tech. B,* **1**, pp. 376-378, 1983.

Wang, K.L. and P.G. Yuh, "Theory and Applications of Band-Aligned Superlattices", *IEEE Jour. Quan. Electron.*, **25**, pp. 12-19, 1989.

Weisbuch, C, B. Vinter, "Quantum well semiconductor structures: Fundamentals and applications", pp. 13-14, 1989.

West, L.C. and S.J. Eglash, "First observation of an extremely large-dipole infrared transition within the conduction band of a GaAs quantum well", *Appl. Phys. Lett.*, **46**, pp. 1156-1158, 1985.

Yariv, A., *Optical Electronics in Modern Communications*, pp. 162, Oxford University Press, 1997

Yu, L.S. and S.S. Li, "A metal grating coupled bound-to-miniband and transition GaAs multiquantum well/superlattice infrared detector", *Appl. Phys. Lett.*, **59**, pp. 1332-1334, 1991.

Yuh, P.F. and K.L. Wang, "Optical transitions in a step quantum well", *Jour. Appl. Phys.*, **65**, pp. 4377-4381, 1989.

THIS PAGE INTENTIONALLY LEFT BLANK

INITIAL DISTRIBUTION LIST

1.   Defense Technical Information Center
      Ft. Belvoir, Virginia

2.   Dudley Knox Library
      Naval Postgraduate School
      Monterey, California

3.   Chairman (Code PH)
      Department of Physics
      Naval Postgraduate School
      Monterey, California

4.   Gamani Karunasiri
      Naval Postgraduate School
      Monterey, California

5.   James Luscombe
      Naval Postgraduate School
      Monterey, California

6.   Kara Harp Okulu Komutanligi
      06100 Bakanliklar
      Ankara, Turkey

7.   Atakan Konukbay
      7nci C. 20nci S. No:8/8
      06500 Bahcelievler
      Ankara, Turkey